
Fine-Tuning of Continuous-Time Diffusion Models as Entropy-Regularized Control

Masatoshi Uehara ^{*}

Genentech

ueharam1@gene.com

Yulai Zhao ^{*}

Princeton University

yulaiz@princeton.edu

Kevin Black

University of California, Berkeley

kvablock@berkeley.edu

Ehsan Hajiramezanali

Genentech

hajiramm@gene.com

Gabriele Scalia

Genentech

scaliag@gene.com

Nathaniel Lee Diamant

Genentech

diamannl@gene.com

Alex M Tseng

Genentech

tsenga5@gene.com

Tommaso Biancalani [†]

Genentech

biancalt@gene.com

Sergey Levine [†]

University of California, Berkeley

sergey.levine@berkeley.edu

Abstract

Diffusion models excel at capturing complex data distributions, such as those of natural images and proteins. While diffusion models are trained to represent the distribution in the training dataset, we often are more concerned with other properties, such as the aesthetic quality of the generated images or the functional properties of generated proteins. Diffusion models can be finetuned in a goal-directed way by maximizing the value of some reward function (e.g., the aesthetic quality of an image). However, these approaches may lead to reduced sample diversity, significant deviations from the training data distribution, and even poor sample quality due to the exploitation of an imperfect reward function. The last issue often occurs when the reward function is a learned model meant to approximate a ground-truth “genuine” reward, as is the case in many practical applications. These challenges, collectively termed “reward collapse,” pose a substantial obstacle. To address this reward collapse, we frame the finetuning problem as entropy-regularized control against the pretrained diffusion model, i.e., directly optimizing entropy-enhanced rewards with neural SDEs. We present theoretical and empirical evidence that demonstrates our framework is capable of efficiently generating diverse samples with high genuine rewards, mitigating the overoptimization of imperfect reward models.

1 Introduction

Diffusion models have gained widespread adoption as effective tools for modeling complex distributions (Sohl-Dickstein et al., 2015; Song et al., 2020; Ho et al., 2020). These models have demonstrated state-of-the-art performance in various domains such as image generation and biological sequence generation (Jing et al., 2022; Wu et al., 2022). While diffusion models effectively capture complex data distributions, our primary goal frequently involves acquiring a finely tuned sampler customized for a specific task using the pre-trained diffusion model as a foundation. For instance, in image generation, we might like to fine-tune diffusion models to enhance aesthetic quality. In biology, we might aim to improve bioactivity. Recent endeavors have pursued this objective through reinforcement learning (RL) (Fan et al., 2023; Black et al., 2023) as well as direct backpropagation through

^{*}Equal contributions

[†]Corresponding authors

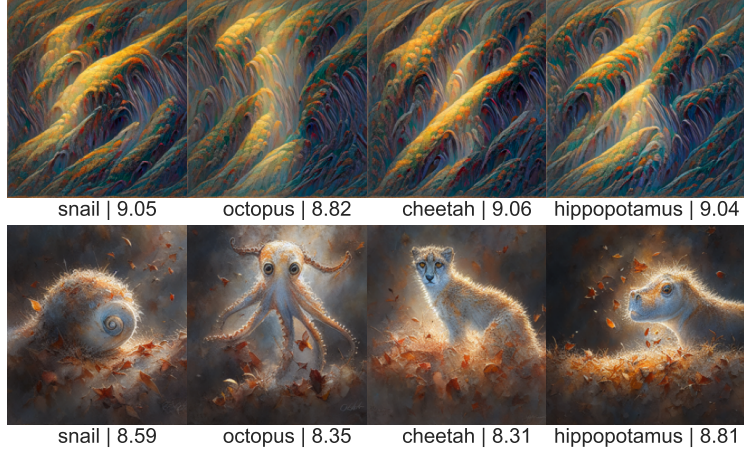


Figure 1: **Mitigating nominal reward exploitation with entropy-regularized control.** Diffusion models fine-tuned in a goal-directed manner can produce images (top) with high nominal reward values such as aesthetic scores. However, these images lack realism because the naive fine-tuning process is not incentivized to stay close to the pre-trained data distribution. Our approach (bottom) mitigates this issue via entropy-regularized stochastic optimal control.

differentiable reward functions (Clark et al., 2023; Prabhudesai et al., 2023). Such reward functions are typically learned models meant to approximate a ground-truth “genuine” reward; e.g., an aesthetic classifier is meant to approximate the true aesthetic preferences of human raters.

While these methods allow us to generate samples with high “nominal” (approximate) rewards, they often suffer from reward collapse. Reward collapse manifests as fine-tuned models produce the same samples with low genuine rewards, as illustrated in Figure 1. This issue arises because nominal rewards are usually learned from a finite number of training data to approximate the genuine reward function, meaning that they are accurate only within their training data distribution. Consequently, fine-tuning methods quickly exploit nominal rewards by moving beyond the support of this distribution. Even ignoring nominal reward exploitation, reward collapse is problematic because diversity is, in itself, a desirable property of generative models. For example, we typically expect generative models to generate diverse candidates of protein sequences to run good wet lab experiments (Watson et al., 2022).

Our goal is to develop a principled algorithmic framework for fine-tuning diffusion models that both optimizes a user-specified reward function and captures a diverse distribution that stays close to the training data, thus alleviating reward collapse issues. To achieve this, we frame the fine-tuning of diffusion models as an entropy-regularized control problem. It is known that diffusion models can be formulated as stochastic differential equations (SDEs) with a drift term and a diffusion term (Song et al., 2020). Based on this formulation, in a fine-tuning step, we consider solving stochastic control by neural SDEs in a computationally efficient manner. Here, we introduce a loss that combines a terminal reward with entropy regularization against the pre-trained diffusion model, with respect to both a drift term and an initial distribution. This entropy-regularization term enables us to maintain the bridges (i.e., the posterior distributions of trajectories conditioned on a terminal point) of pre-trained diffusion models, akin to bridge-matching generative models (Shi et al., 2023), such that the fine-tuned diffusion model avoids deviating too much from the pre-trained diffusion model.

Notably, we formally show that the fine-tuned SDE, optimized for both the drift term and initial distribution, can produce specific distributions with high diversity and high nominal rewards that are within the support of their training data distribution. Hence, our approach effectively mitigates the reward-collapse problem since nominal rewards accurately approximate genuine rewards in that region.

Our contribution can be summarized as follows: we introduce a computationally efficient, theoretically and empirically supported method for fine-tuning diffusion models: **ELEGANT** (finE-tuning douBLe Entropy reGulArized coNTrol) that excels at generating samples with both high genuine rewards and a high degree of diversity. While existing techniques in image generation (Fan et al.,

2023; Prabhudesai et al., 2023; Clark et al., 2023) include components for mitigating reward collapse, we demonstrate stronger theoretical support (among methods that directly backpropagate through differentiable rewards) and superior empirical performance (compared to a KL-penalized RL approach). Additionally, unlike prior work, we apply our method to both image generation and biological sequence generation, demonstrating its effectiveness across multiple domains.

2 Related Works

We provide an overview of related works. We leave the discussion of our work, including fine-tuning LLMs, sampling with control methods, and MCMC methods to Appendix A.

Diffusion models. Denoising diffusion probabilistic models (DDPMs) create a dynamic stochastic transport using SDEs, where the drift aligns with a specific score function (Song et al., 2020). The impressive performance of DDPMs has spurred the recent advancements in bridge (flow)-matching techniques, which construct stochastic transport through SDEs with drift terms aligned to specific bridge functions (Shi et al., 2023; Tong et al., 2023; Lipman et al., 2023; Somnath et al., 2023; Liu et al., 2023; Delbracio and Milanfar, 2023). For a more comprehensive review, we direct readers to Shi et al. (2023). Note our that fine-tuning methods are applicable to any model with diffusion terms, but are not suitable for ODE-based models such as flow models (Papamakarios et al., 2021).

Guidance. Dhariwal and Nichol (2021) introduced classifier-based guidance, an inference-time technique for steering diffusion samples towards a particular class. More generally, guidance uses an auxiliary differentiable objective (e.g., a neural network) to steer diffusion samples towards a desired property (Graikos et al., 2022; Bansal et al., 2023). In our experiments, we show that our fine-tuning technique outperforms a guidance baseline that uses the gradients of the reward model to steer the pre-trained diffusion model toward high-reward regions.

Fine-tuning as RL/control. Lee et al. (2023); Wu et al. (2023) employ supervised learning techniques to optimize reward functions, while Black et al. (2023); Fan et al. (2023) employ an RL-based method to achieve a similar goal. Clark et al. (2023); Xu et al. (2023); Prabhudesai et al. (2023) present a fine-tuning method that involve direct backpropagation with respect to rewards, which bears some resemblance to our work. Nevertheless, there are several notable distinctions between our approaches. Specifically, we incorporate an entropy-regularization term and also learn an initial distribution, both of which play a critical role in targeting the desired distribution. We present novel theoretical results that demonstrate the benefits of our approach, and we provide empirical evidence that our method more efficiently mitigates reward collapse.

3 Preliminaries

We briefly review current continuous-time diffusion models. A diffusion model is described by the following SDE:

$$dx_t = f(t, x_t)dt + \sigma(t)dw_t, \quad x_0 \sim \nu_{\text{ini}} \in \Delta(\mathbb{R}^d), \quad (1)$$

where $f : [0, T] \times \mathbb{R}^d \rightarrow \mathbb{R}^d$ is a drift coefficient, and $\sigma : [0, T] \rightarrow \mathbb{R}_{>0}$ is a diffusion coefficient associated with a d -dimensional Brownian motion w_t , and ν_{ini} is an initial distribution such as a Gaussian distribution. Note that many papers use the opposite convention, with $t = T$ corresponding to the initial distribution and $t = 0$ corresponding to the data. When training diffusion models, the goal is to learn $f(t, x_t)$ from the data at hand so that the generated distribution from the SDE (1) corresponds to the data distribution through score matching (Song et al., 2020) or bridge matching (Shi et al., 2023). For details, refer to Appendix D.

In our work, we focus on scenarios where we have such a pre-trained diffusion model (i.e., a pre-trained SDE). Denoting the density at time T induced by the pre-trained SDE in (1) as $p_{\text{data}} \in \Delta(\mathbb{R}^d)$, this p_{data} captures the intricate structure of the data distribution. In image generation, p_{data} captures the structure of natural images, while in biological sequence generation, it captures the biological space.

Notation. We often consider a measure \mathbb{P} induced by an SDE on $\mathcal{C} := C([0, T], \mathbb{R}^d)$ where $C([0, T], \mathbb{R}^d)$ is the whole set of continuous functions mapping from $[0, T]$ to \mathbb{R}^d (Karatzas and Shreve, 2012). The notation $\mathbb{E}_{\mathbb{P}}[f(x_{0:T})]$ means that the expectation is taken for $f(\cdot)$ w.r.t. \mathbb{P} . We denote \mathbb{P}_t as the marginal distribution over \mathbb{R}^d at time t , $\mathbb{P}_{s,t}(x_s, x_t)$ the joint distribution over \mathbb{R}^d time s and t , and $\mathbb{P}_{s|t}(x_s | x_t)$ the conditional distribution at time s given time t . We also denote the

distribution of the process pinned down at an initial and terminal point x_0, x_T by $\mathbb{P}_{\cdot|0,T}(\cdot|x_0, x_T)$ (we similarly define $\mathbb{P}_{\cdot|T}(\cdot|x_T)$). With a slight abuse of notation, we exchangeably use distributions and densities³

We defer all proofs to Appendix C.

4 Desired Properties for Fine-Tuning

In this section, we elucidate the desired properties for methods that fine-tune diffusion models.

In the presence of a reward function $r : \mathbb{R}^d \rightarrow \mathbb{R}$, such as aesthetic quality in image generation or bioactivity in biological sequence generation, our aim might be to fine-tune a pre-trained diffusion model so as to maximize this reward function, for example to generate images that are more aesthetically pleasing.

However, the “genuine” reward function (e.g., a true human rating of aesthetic appearance) is usually unknown, and instead a computational proxy must be learned from data — typically from the same or a similar distribution as the pre-training data for the diffusion model. As a result, while $r(x)$ may be close to the genuine reward function within the support of p_{data} , it might not be accurate outside of this domain. More formally, by denoting the genuine reward by r^* , a nominal reward r is typically learned as

$$r = \operatorname{argmin}_{r' \in \mathcal{F}} \sum_i \{r^*(x^{(i)}) - r'(x^{(i)})\}^2,$$

where $\{x^{(i)}, r^*(x^{(i)})\}_{i=1}^n$ is a dataset, and \mathcal{F} is a function class (e.g., neural networks) mapping from \mathbb{R}^d to \mathbb{R} . Under mild conditions, it has been shown that in high probability, the mean square error on p_{data} is small, i.e.,

$$\mathbb{E}_{x \sim p_{\text{data}}}[\{r^*(x) - r(x)\}^2] = O(\sqrt{\operatorname{Cap}(\mathcal{F})/n}),$$

where $\operatorname{Cap}(\mathcal{F})$ is a capacity of \mathcal{F} (Wainwright, 2019). However, this does not hold outside of the support of p_{data} .

Taking this into account, we aim to fine-tune a diffusion model in a way that preserves three essential properties: (a1) the ability to generate samples with high rewards, (a2) maintaining the diversity of samples, and (a3) ensuring sufficient proximity to the initial pre-trained diffusion (1). In particular, (a3) helps avoid overoptimization because learned reward functions tend to be accurate on the support of p_{data} .

To accomplish this, we consider the optimization problem:

$$p_{\text{tar}} = \operatorname{argmax}_{p \in \Delta(\mathbb{R}^d)} \underbrace{\mathbb{E}_{x \sim p}[r(x)]}_{\Psi(1)} - \alpha \underbrace{\operatorname{KL}(p \| p_{\text{data}})}_{\Psi(2)}, \quad (2)$$

where $\alpha \in \mathbb{R}_{>0}$ is a hyperparameter. The initial reward term $\Psi(1)$ is intended to uphold the property (a1), while the second entropy term $\Psi(2)$ is aimed at preserving the property (a2). To achieve (a2), one might consider just adding a relative entropy against a uniform distribution. However, in our case, we add the relative entropy against p_{data} to maintain property (a3).

It can be shown that the target distribution in (2) takes the following analytical form:

$$p_{\text{tar}}(x) = \exp(r(x)/\alpha) p_{\text{data}}(x) / C_{\text{tar}}, \quad (3)$$

where C_{tar} is a normalizing constant. Therefore, the aim of our method is to provide a tractable and theoretically principled way to emulate p_{tar} as a fine-tuning step.

4.1 Importance of KL Regularization

Before explaining our approach to sample from p_{tar} , we elucidate the necessity of incorporating entropy regularization term in (2). This can be seen by examining the limit cases as α tends towards 0 and when we fix $\alpha = 0$ a priori. To be more precise, as α approaches zero, p_{tar} tends to converge to a Dirac delta distribution at x_{tar}^* , defined by:

$$x_{\text{tar}}^* = \operatorname{argmax}_{x \in \mathbb{R}^d: p_{\text{data}}(x) > 0} r(x).$$

³We sometimes denote densities such as $d\mathbb{P}_T/d\mu$ by just \mathbb{P}_T where μ is Lebesgue measure.

This x_{tar}^* represents an optimal x within the support of p_{data} . Conversely, if we directly solve (2) with $\alpha = 0$, we may venture beyond the support:

$$x^* = \operatorname{argmax}_{x \in \mathbb{R}^d} r(x).$$

This implies that the generated samples might no longer adhere to the characteristics of natural images in image generation or biological sequences within the biological space. As we mentioned, since $r(x)$ is typically a learned reward function from the data, it won't be accurate outside of the support of $p_{\text{data}}(x)$. Hence, x^* would not have a high genuine reward, which results in “overoptimization”. For example, this approach results in the unnatural but high nominal reward images in Figure 1.

Remark 1 (Failure of naïve approach). *The score function of $p_{\text{tar}}(\cdot)$ w.r.t. x is given by $\nabla r(x)/\alpha + \nabla \log p_{\text{data}}(x)$. Therefore, some readers might question whether we can straightforwardly use:*

$$dx_t = \{f(t, x_t) + \nabla r(x_t)/\alpha\}dt + \sigma(t)dw_t$$

However, there is no validity of this approach because we cannot simply use $\nabla r(x)$ for time $t \neq T$. We will see a correct approach in Lemma 2.

5 Entropy-Regularized Control with Pre-Trained Models

We show how to sample from the target distribution p_{tar} using entropy-regularized control and a pre-trained model.

5.1 Stochastic Control Formulation

To fine-tune diffusion models, we consider the following SDE by adding an additional drift term u and changing the initial distribution of (1):

$$dx_t = \{f(t, x_t) + u(t, x_t)\}dt + \sigma(t)dw_t, x_0 \sim \nu, \quad (4)$$

where $u(\cdot, \cdot) : [0, T] \times \mathbb{R}^d \rightarrow \mathbb{R}$ is a drift coefficient we want to learn and $\nu \in \Delta(\mathbb{R}^d)$ is an initial distribution we want to learn. When $u = 0$ and $\nu = \nu_{\text{ini}}$, this reduces to a pre-trained SDE in (1). Our objective is to select u and ν in such a way that the density at time T , induced by this SDE, corresponds to p_{tar} .

Now, let's turn our attention to the objective function designed to achieve this objective. Being motivated by (2), the objective function we consider is as follows:

$$\begin{aligned} u^*, \nu^* &= \operatorname{argmax}_{u, \nu} \mathbb{E}_{\mathbb{P}^{u, \nu}} \left[\underbrace{r(x_T)}_{(b1)} \right] \\ &\quad - \underbrace{\frac{\alpha}{2} \mathbb{E}_{\mathbb{P}^{u, \nu}} \left[\int_{t=0}^T \frac{\|u(t, x_t)\|^2}{\sigma^2(t)} dt + \log \left(\frac{\nu(x_0)}{\nu_{\text{ini}}(x_0)} \right) \right]}_{(b2)} \end{aligned} \quad (5)$$

where $\mathbb{P}^{u, \nu}$ is a measure over \mathcal{C} induced by the SDE (4) associated with (u, ν) . Within this equation, component (b1) is introduced to obtain samples with high rewards. This is equal to $\Psi(1)$ in (2) when $p(\cdot)$ in (2) comes from $\mathbb{P}_T^{u, \nu}$. The component (b2) corresponds to the KL divergence over trajectories: $\text{KL}(\mathbb{P}^{u, \nu}(\cdot) \parallel \mathbb{P}^{\text{data}}(\cdot))$ where \mathbb{P}^{data} is a measure over \mathcal{C} induced by the pre-trained SDE (1). This is actually equal to $\Psi(2)$ in (2) as we will see in the proof of our key theorem soon.

We can derive an explicit expression for the marginal distribution at time t under the distribution over \mathcal{C} induced by the SDE associated with the optimal drift and initial distribution denoted by \mathbb{P}^* (i.e., \mathbb{P}^{u^*, ν^*}). Here, we define the optimal (entropy-regularized) value function as

$$v_t^*(x) = \mathbb{E}_{\mathbb{P}^*} \left[r(x_T) - \frac{\alpha}{2} \int_{k=t}^T \frac{\|u(k, x_k)\|^2}{\sigma^2(k)} dk \mid x_t = x \right].$$

Theorem 1 (Induced marginal distribution). *The marginal density at step $t \in [0, T]$ under the diffusion model with a drift term u^* and a diffusion coefficient ν^* (i.e., \mathbb{P}_t^*) is*

$$\mathbb{P}_t^*(\cdot) = \exp(v_t^*(x)/\alpha) \mathbb{P}_t^{\text{data}}(x) / C_{\text{tar}} \quad (6)$$

where $\mathbb{P}_t^{\text{data}}(\cdot)$ is a marginal distribution at t of \mathbb{P}^{data} .

This marginal density comprises two components: the optimal value function term and the density at time t induced by the pre-trained diffusion model. Note that the normalizing constant C_{tar} is independent of t .

Crucially, as a corollary, we observe that by generating a sample following the SDE (4) with (u^*, ν^*) , we can sample from the target p_{tar} at the final time step T . Furthermore, we can also determine the explicit form of ν^* .

Corollary 1 (Justification of control problem).

$$\mathbb{P}_T(\cdot) = p_{\text{tar}}(\cdot).$$

Corollary 2 (Optimal initial distribution).

$$\nu^*(\cdot) = \exp(v_0^*(\cdot)/\alpha) \nu_{\text{ini}}(\cdot)/C_{\text{tar}}.$$

In the following section, to gain deeper insights, we explore two interpretations.

5.2 Feynman–Kac Formulation

We see an interpretable formulation of the optimal value function. We use this form to learn the optimal initial distribution later in our algorithm and the proof of Theorem 1.

Lemma 1 (Feynman–Kac Formulation).

$$\exp\left(\frac{v_t^*(x)}{\alpha}\right) = \mathbb{E}_{\mathbb{P}^{\text{data}}} \left[\exp\left(\frac{r(x_T)}{\alpha}\right) | x_t = x \right].$$

This lemma illustrates that the value function at (t, x) is higher when it allows us to hit regions with high rewards at $t = T$ by following the pre-trained diffusion model afterward. Using this optimal value function, we can write the optimal drift $u^*(t, x)$ as $\sigma^2(t) \nabla_x v_t^*(x)/\alpha$. By plugging Lemma 1 into $\sigma^2(t) \nabla_x v_t^*(x)/\alpha$, we obtain the following.

Lemma 2 (Optimal drift).

$$u^*(t, x) = \sigma^2(t) \nabla_x \left\{ \log \mathbb{E}_{\mathbb{P}^{\text{data}}} \left[\exp\left(\frac{r(x_T)}{\alpha}\right) | x_t = x \right] \right\}.$$

It says the optimal control aims to move the current state x at time t toward a point where it becomes easier to achieve higher rewards after following the pre-trained diffusion.

Note that this equals $\nabla_x r(x)/\alpha$ when $t = T$, but not at $t < T$. Therefore, the straightforward approach in Remark 1 does not work. With certain approximation, this becomes

$$u^*(t, x) \approx \sigma^2(t)/\alpha \mathbb{E}_{\mathbb{P}^{\text{data}}} [r(x_T) | x_t = x].$$

This formulation has a close connection with classifier guidance (Dhariwal and Nichol, 2021). For more details, refer to Appendix B.

5.3 Bridge Preserving Property

We start by exploring more explicit representations of joint and conditional distributions to deepen the understanding of our control problem.

Lemma 3 (Joint distributions). *Let $0 \leq s < t \leq T$. Then,*

$$\begin{aligned} \mathbb{P}_{s,t}^*(x, y) &= \mathbb{P}_{s,t}^{\text{data}}(x, y) \exp(v_t^*(y)/\alpha)/C_{\text{tar}}, \\ \mathbb{P}_{s|t}^*(x|y) &= \mathbb{P}_{s|t}^{\text{data}}(x|y). \end{aligned} \tag{7}$$

Interestingly, in (7), the posterior distributions of pre-trained SDE and optimal SDE are identical. This property is a result of the entropy-regularized term. This theorem can be generalized further.

Lemma 4 (Bridge perseverance). *Let $\mathbb{P}_{\cdot|T}^*(\cdot|x_T), \mathbb{P}_{\cdot|T}^{\text{data}}(\cdot|x_T)$ be distributions of \mathbb{P}^* , \mathbb{P}^{data} conditioned on states at terminal T , respectively. Then,*

$$\mathbb{P}_{\cdot|T}^*(\cdot|x_T) = \mathbb{P}_{\cdot|T}^{\text{data}}(\cdot|x_T).$$

As an immediate corollary, we also obtain $\mathbb{P}_{|0,T}^*(\cdot) = \mathbb{P}_{|0,T}^{\text{data}}(\cdot)$. These posterior distributions are often referred to as bridges. Note that in bridge matching methods, generative models are trained to align the bridge with the reference Brownian bridge while maintaining the initial distribution as ν_{ini} and the terminal distribution as p_{data} (Shi et al., 2023). Our fine-tuning method can be viewed as a bridge-matching *fine-tuning* approach between 0 and T while keeping the terminal distribution as $\exp(r(x)/\alpha)p_{\text{data}}(x)/C_{\text{tar}}$. This bridge-matching property is valuable in preventing samples from going beyond the support of p_{data} .

6 Learning an Optimal Initial Distribution via Entropy-Regularized Control

Up to this point, we have illustrated that addressing the stochastic control problem enables the creation of generative models for the target density p_{tar} . Existing literature on neural ODE/SDEs (Chen et al., 2018; Li et al., 2020; Tzen and Raginsky, 2019) has established that these control problems can be effectively solved by relying on the expressive power of a neural network, and employing sufficiently small discretization steps.

Although it seems plausible to employ any neural SDE solver for solving stochastic control problems (5), in typical algorithms, the initial point is fixed. Even when the initial point is unknown, it is commonly assumed to follow a Dirac delta distribution. In contrast, our control problem in Eq. (5) necessitates the learning of a stochastic initial distribution, which can function as a sampler.

A straightforward way involves assuming a Gaussian model with a mean parameterized by a neural network. While this approach is appealingly simple, it may lead to significant misspecification when ν^* is a multi-modal distribution.

To address this challenge, we once again turn to approximating ν^* using an SDE, as SDE-induced distributions have the capability to represent intricate multi-modal distributions. We start with a reference SDE over the interval $[-T, 0]$:

$$t \in [-T, 0]; dx_t = \tilde{\sigma}(t)dw_t, x_{-T} = x_{\text{fix}},$$

such that the distribution at time 0 follows ν_{ini} . Given that ν_{ini} is typically simple (e.g., $\mathcal{N}(0, \mathbb{I}_d)$), it is usually straightforward to construct such an SDE with a diffusion coefficient $\tilde{\sigma} : [0, T] \rightarrow \mathbb{R}$.

Building upon this baseline SDE, we introduce another SDE over the same interval $[-T, 0]$:

$$dx_t = q(t, x_t)x_t + \tilde{\sigma}(t)dw_t, x_{-T} = x_{\text{fix}}. \quad (8)$$

where $q : [-T, 0] \times \mathbb{R}^d \rightarrow \mathbb{R}$. This time, we aim to guide a drift coefficient q over this interval $[-T, 0]$ such that the distribution at 0 follows ν^* . Specifically, we formulate the following stochastic control problem:

$$q^* = \operatorname{argmax}_q \mathbb{E}_{\mathbb{P}^q} \left[v_0^*(x_0) - \frac{\alpha}{2} \int_{-T}^0 \frac{\|q(t, x_t)\|^2}{\tilde{\sigma}^2(t)} dt \right], \quad (9)$$

where \mathbb{P}^q represents the measure induced by the SDE (8) with a drift coefficient q .

Theorem 2 (Justification of the second control problem). *The marginal density at time 0 induced by the SDE (8) with the drift q^* , i.e., $\mathbb{P}_0^{q^*}(\cdot)$, is $\nu^*(\cdot)$*

This shows that by solving (9) and following the learned SDE from $-T$ to 0, we can sample from ν^* at time 0.

7 Algorithm

We are ready to present our method, **ELEGANT**, which is fully described in Algorithm 1. The algorithm consists of 3 steps:

1. Learn the value function $v_0^*(x)$, which we will discuss in Section 7.1.
2. Solve the stochastic control (10) with a neural SDE solver using the learned $v_0^*(x)$ in the first step.
3. Solve the stochastic control (11) with a neural SDE using the learned ν^* in the second step (i.e., $\hat{\nu}$). Compared to (5), we fix the initial distribution as $\hat{\nu}$.

For our neural SDE solver, we use a standard oracle in Algorithm 3 as in Kidger et al. (2021); Chen et al. (2018). A detailed implementation is described in Appendix E.1. To solve (10), we use the following parametrization:

$$\begin{aligned} z_t &:= [x_t^\top, y_t]^\top \in \mathbb{R}^{d+1}, L := -y_0 + \hat{a}(x_0), z_{\text{ini}} := x_{\text{fix}} \\ \bar{f} &:= [q^\top, -0.5\alpha\|q\|^2/\tilde{\sigma}^2]^\top, \bar{g} := [\tilde{\sigma}\mathbf{1}_d, 0]^\top \end{aligned}$$

Similarly, to solve (11), we can use this solver with the following parametrization:

$$\begin{aligned} z_t &:= [x_t^\top, y_t]^\top \in \mathbb{R}^{d+1}, L := -y_T + r(x_T), z_{\text{ini}} := \hat{\nu} \\ \bar{f} &:= [\{f + u\}^\top, -0.5\alpha\|u\|^2/\sigma^2]^\top, \bar{g} := [\sigma\mathbf{1}_d, 0]^\top. \end{aligned}$$

Finally, after learning the drift terms \hat{q} and \hat{u} , during the sampling phase, we follow the learned SDE (Algorithm 2).

Algorithm 1 ELEGANT (finE-tuning douBLe Entropy reGulArized coNTrol)

- 1: **Require:** Parameter $\alpha \in \mathbb{R}^+$, a pre-trained diffusion model with drift coefficient $f : [0, T] \times \mathbb{R}^d \rightarrow \mathbb{R}$ and diffusion coefficient $\sigma : [0, T] \rightarrow \mathbb{R}$, a base coefficient $\tilde{\sigma} : [-T, 0] \rightarrow \mathbb{R}$ and a base initial point x_{fix} .
- 2: Learn an optimal value function at $t = 0$ (i.e., v_0^*) and denote it by $\hat{a} : \mathbb{R}^d \rightarrow \mathbb{R}$ invoking **Algorithm 4**.
- 3: Using a neural SDE solver (**Algorithm 3**), solve

$$\hat{q} = \operatorname{argmax}_q \mathbb{E}_{\mathbb{P}^q} \left[\hat{a}(x_0) - \frac{\alpha}{2} \int_{-T}^0 \frac{\|q(t, x_t)\|^2}{\tilde{\sigma}^2(t)} dt \right]. \quad (10)$$

- 4: Let $\hat{\nu}$ be a distribution at $t = 0$ following the SDE:

$$dx_t = \hat{q}(t, x_t)dt + \tilde{\sigma}(t)dw_t, x_{-T} = x_{\text{fix}}.$$

- 5: Using a neural SDE solver (**Algorithm 3**), solve

$$\hat{u} = \operatorname{argmax}_u \mathbb{E}_{\mathbb{P}^u, \hat{\nu}} \left[r(x_T) - \frac{\alpha}{2} \int_{t=0}^T \frac{\|u(t, x_t)\|^2}{\sigma^2(t)} dt \right]. \quad (11)$$

- 6: **Output:** Drift coefficients \hat{q}, \hat{u}

Algorithm 2 Fine-Tuned Sampler

- 1: From $-T$ to 0, follow the SDE:

$$dx_t = \hat{q}(t, x_t)dt + \tilde{\sigma}(t)dw_t, x_{-T} = x_{\text{fix}}$$

- 2: From 0 to T , follow the SDE:

$$dx_t = \{f(t, x_t) + \hat{u}(t, x_t)\}dt + \sigma(t)dw_t.$$

- 3: **Output:** x_T

Algorithm 3 NeuralSDE Solver

- 1: **Input:** A diffusion coefficient $\bar{g} : [0, T] \rightarrow \mathcal{Z}$, a loss function $L : \mathcal{Z} \rightarrow \mathbb{R}$, an initial distribution $\bar{\nu}$
- 2: Solve the following and denote the solution by f^\dagger :

$$\operatorname{argmax}_{\bar{f} : [0, T] \times \mathcal{Z} \rightarrow \mathcal{Z}} L(z_T), dz_t = \bar{f}(t, z_t)dt + \bar{g}(t)dw_t, z_0 \sim z_{\text{ini}}.$$

- 3: **Output:** f^\dagger

7.1 Value Function Estimation

In the initial stage of **ELEGANT**, our objective is to learn $v_0^*(x_0)$. To achieve this, we use the following:

$$v_0^*(x) = \alpha \log(\mathbb{E}_{\mathbb{P}^{\text{data}}}[\exp(r(x_T)/\alpha) | x_0 = x]),$$

which is obtained as a corollary of Lemma 1 at $t = 0$. Then, by taking a differentiable function class $\mathcal{A} : \mathbb{R}^d \rightarrow \mathbb{R}$, we can use an empirical risk minimization (ERM) algorithm to regress $\exp(r(x_T)/\alpha)$ on x_0 .

While the above procedure is mathematically sound, in practice, where α is small, it may face numerical instability. We instead recommend the following alternative. Suppose $r(x_T) = k(x_0) + \epsilon$ where ϵ is noise under \mathbb{P}^{data} . Then,

$$v_0^*(x) = k(x) + \alpha \log \mathbb{E}_{\mathbb{P}^{\text{data}}}[\exp(\epsilon/\alpha) | x_0 = x].$$

Therefore, we can directly regress $r(x_T)$ on x_0 since the difference between $k(x)$ and $v_0^*(x)$ remains constant. The complete algorithm is in Algorithm 4. For more advanced methods, refer to Appendix E.2.

Algorithm 4 Optimal Value Function Estimation

- 1: **Input:** Function class $\mathcal{A} \subset [\mathbb{R}^d \rightarrow \mathbb{R}]$
- 2: Generate a dataset \mathcal{D} that consists of pairs of (x, y) : $x \sim \nu_{\text{ini}}$ and y as $r(x_T)$ following the pre-trained SDE:

$$dx_t = f(t, x_t)dt + \sigma(t)dw_t.$$

- 3: Run an empirical risk minimization:

$$\hat{a} = \operatorname{argmin}_{a \in \mathcal{A}} \sum_{(x, y) \sim \mathcal{D}} \{\hat{a}(x) - y\}^2.$$

- 4: **Output:** \hat{a}

7.2 Sources of Approximation Errors

Lastly, we explain the factors contributing to approximation errors in our algorithm. First, our method relies on the precision of neural SDE solvers, specifically, the expressiveness of neural networks and errors from discretization (Tzen and Raginsky, 2019). Similarly, in the sampling phase, we also incur errors stemming from discretization. Additionally, our method relies on the expressiveness of another neural network in value function estimation.

8 Experiments

We compare **ELEGANT** against several baselines across two domains. Our goal is to check that **ELEGANT** enables us to obtain diffusion models that generate high-reward samples while avoiding reward collapse and preserving diversity. We will begin by providing an overview of the baselines, describing the experimental setups, and specifying the evaluation metrics employed across all three domains. For more detailed information on each experiment, including dataset, architecture, and hyperparameters, refer to Appendix F.

Methods to compare. We compare the following:

- **ELEGANT**: Our method.
- **NO KL**: This is **ELEGANT** without the KL regularization and initial distribution learning. This essentially corresponds to AlignProp (Prabhudesai et al., 2023) and DRAFT (Clark et al., 2023) in the discrete-time formulation. While several ways to mitigate reward collapse in these papers are discussed, we will compare them with our work later in Section 8.2.
- **PPO + KL**: KL-penalized RL finetuning with PPO (Schulman et al., 2017). This is an improved version of both DPOK (Fan et al., 2023) and DDPO (Black et al., 2023) with a KL penalty applied to the rewards. For details, refer to Appendix E.3.
- **Guidance**: We train a reward model to predict the reward value y from a sample x . We use this model to guide the sampling process (Dhariwal and Nichol, 2021; Graikos et al., 2022) toward high rewards. For details, refer to Appendix E.3.

Experiment setup. In all scenarios, we start by preparing a diffusion model with a standard dataset, containing a mix of high- and low-reward samples. Then, we create a (nominal) reward function r by training a neural network reward model on a dataset with reward labels $\{x^{(i)}, r^*(x^{(i)})\}_{i=1}^n$, ensuring that r closely approximates the “genuine” reward function r^* on the data distribution of the dataset (i.e., on the support of pre-trained diffusion model). Following existing work, we mostly evaluate performance in terms of r , and measure reward collapse using separate divergence and diversity metrics (except for one task, where r^* is known).

Evaluation. We record the reward $r(x_T)$ ((b1) in Equation (5)), the KL divergence term ((b2) in Equation (5)), and a measure of diversity among generated samples, defined as $\mathbb{E}_{x \sim p, z \sim p}[d(x, z)]$, where $d(x, z)$ represents the distance between x and z . In our results, we present the mean values of the reward (Reward), the KL term (KL-Div), and the diversity term (Div) across several trials.

Our aim is to fine-tune diffusion models so that they have high (Reward), low (KL-div), and high (Div): that is, to produce diverse yet high reward samples from a distribution that stays close to the data. For one of our evaluation tasks (Section 8.2), we know the true function r^* (though it is *not* provided to our algorithm), and therefore can directly measure the degree to which our method mitigates overoptimization by comparing the values of r and r^* for our method and baselines.

Table 1: Results for GFP. We set $\alpha = 0.1$ for **ELEGANT** and **PPO + KL**. We normalize florence scores. Note the pre-trained model has 0.90 (reward), 0.0 (KL-div), and 2.4 (div).

	Reward (r) \uparrow	KL-Div \downarrow	Div \uparrow
Guidance	0.94 ± 0.01	624	2.1
PPO + KL	0.96 ± 0.01	95	2.0
ELEGANT (Ours)	0.98 ± 0.00	32	2.2

Table 2: Results for TFBind. We set $\alpha = 0.005$ for **ELEGANT** and **PPO + KL**. Note the pre-trained model has 0.45 (reward), 0.0 (KL-div), 5.3 (div).

	Reward (r) \uparrow	KL-Div \downarrow	Div \uparrow
Guidance	0.81 ± 0.03	709	2.5
PPO + KL	0.98 ± 0.00	110	2.2
ELEGANT (Ours)	0.98 ± 0.00	82	2.5

Table 3: TFBind. We set $\alpha = 0.01$ for **ELEGANT** and PPO. For **Truncation**, we set $K = 0.8T$. It is seen that **ELEGANT** can circumvent overoptimization while other methods suffer from it.

	Reward (r) \uparrow	Reward (r^*) \uparrow
NO KL	1.0 ± 0.0	0.76 ± 0.02
Guidance	0.81 ± 0.03	0.76 ± 0.03
PPO + KL	0.987 ± 0.001	0.84 ± 0.01
Random	1.0 ± 0.0	0.77 ± 0.01
Truncation	1.0 ± 0.0	0.78 ± 0.01
ELEGANT (Ours)	0.989 ± 0.001	0.88 ± 0.01

However, for the other tasks, we must rely on the (KL-div) and (Div) metrics, as well as qualitative examples, to evaluate this.

8.1 Protein and DNA Sequences

We study two distinct biological sequence tasks: GFP and TFBind (Trabucco et al., 2022). In the GFP task, x represents green fluorescent protein sequences, each with a length of 237, and $r^*(x)$ signifies their fluorescence value (Sarkisyan et al., 2016). In the TFBind task, x represents DNA sequences, each having a length of 8, while $r^*(x)$ corresponds to their binding activity with human transcription factors (Barrera et al., 2016). Using these datasets, we proceed to train transformer-based diffusion models and oracles (details in Appendix F.1). For the distance metric d , following Ghari et al. (2023), we use Levenshtein distance.

Results. To start, we present the performance of the methods in Tables 1 and 2. It’s clear that **ELEGANT** surpasses **PPO + KL** and **Guidance** in terms of rewards, maintains a smaller KL term, and achieves higher diversity scores. It’s worth noting that while there is typically a tradeoff between the reward and KL term, even when fine-tuned diffusion models yield similar rewards, their KL divergences can vary significantly. This implies that, compared to **PPO + KL**, **ELEGANT** effectively minimizes the KL term while maintaining high rewards. This reduced KL term translates to the alleviation of overoptimization, as in Section 8.2.

Secondly, we observe that entropy regularization plays a crucial role in generating diverse samples. Without entropy regularization, **ELEGANT** tends to produce samples with high rewards (in terms of $r(x)$), but the samples are very similar. The introduction of entropy regularization effectively mitigates this collapse problem. To illustrate this, we present histograms of fine-tuned samplers with varying α in Figure 2. It’s noticeable that as α increases, the average reward degrades slightly, but we are able to obtain more diverse samples.

8.2 Quantitative Evaluation of Overoptimization

In TFBind, where we have knowledge of the genuine reward r^* , we conduct a comparison between **ELEGANT** and several baselines, presented in Table 3. It becomes evident that the version without

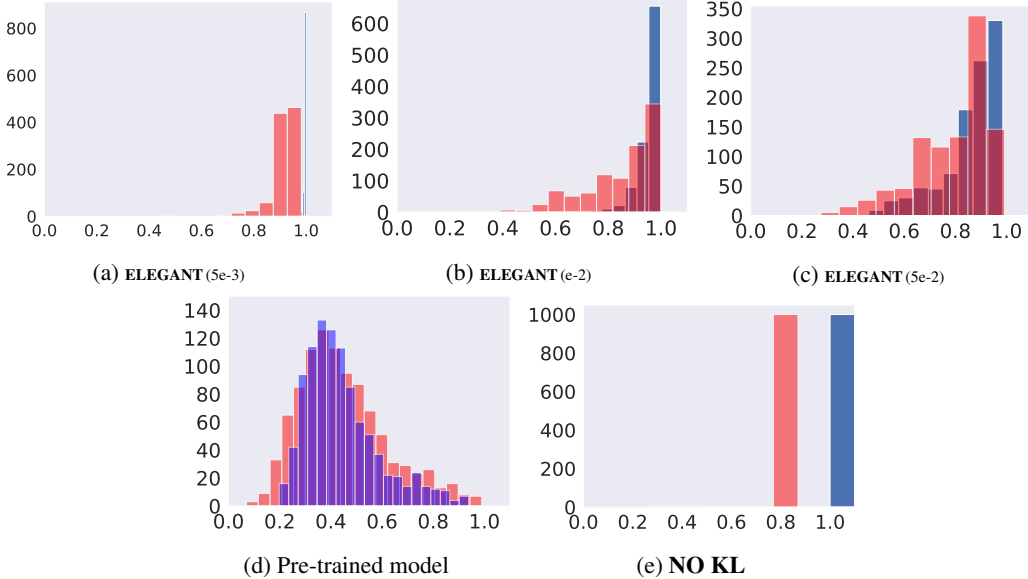


Figure 2: Histograms of 1000 samples generated by fine-tuned diffusions for TFBind in terms of $r^*(x)$ in Red and $r(x)$ in Blue. In **NO KL**, the same sample is generated ($\text{Div} = 0.0$), and it suffers from overoptimization. **ELEGANT** can effectively achieve both high r and r^* . The enlarged figure (a) is in Appendix F.2.2.

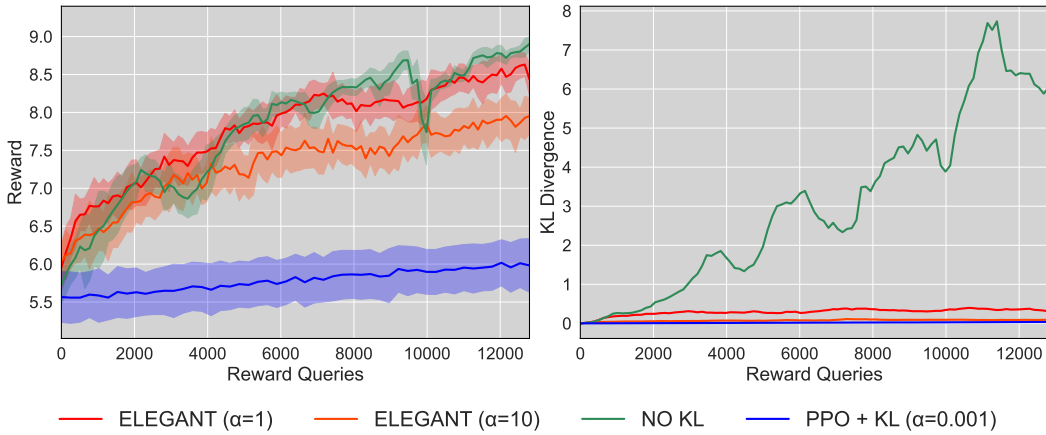


Figure 3: Training curves of reward (left) and KL divergence (right) for fine-tuning aesthetic scores. The x axis corresponds to the number of reward queries in the fine-tuning process. It shows that **ELEGANT** is much faster than PPO, and **ELEGANT** can effectively lower the KL divergence.

KL regularization achieves high values for r , but not for the true reward value r^* . In contrast, our method can overcome overoptimization by effectively minimizing the KL divergence.

In addition, we compare algorithms that focus solely on maximizing $r(x_T)$ (i.e., (b1) in Equation (5)) with several techniques. For instance, the approach presented in Clark et al. (2023) (DRaFT-K) can be adapted to our context by updating drift terms only in the interval $[K, T]$ rather than over the entire interval $[0, T]$ (referred to as **Truncation**). Similarly, AlignProp, as proposed by Prabhudesai et al. (2023), can be applied by randomly selecting the value of K at each epoch (referred to as **Random**). However, in the case of TfBind, it becomes evident that these techniques cannot mitigate overoptimization.



Figure 4: Diverse generated images by **ELEGANT** with high aesthetic scores.

8.3 Images

We use Stable Diffusion v1.5 as the pre-trained diffusion model (Rombach et al., 2022). For $r(x)$, following existing works (Black et al., 2023; Prabhudesai et al., 2023), we use the LAION Aesthetics Predictor V2 (Schuhmann, 2022), which is implemented as a linear MLP model on top of the OpenAI CLIP embeddings (Radford et al., 2021).

Results. We plot the training curves of **ELEGANT** and baselines in Figure 3. First, it can be seen that the training speed of **ELEGANT** is significantly faster than that of **PPO + KL**. Secondly, compared to **NO KL**, the KL divergence curves reveal that **ELEGANT** maintains a consistently lower KL divergence throughout fine-tuning, indicating its ability to generate diverse samples without diverging significantly from the original data distribution. Some generated examples are shown in Figure 4. We defer a more detailed comparison (including guidance) to Appendix F.2.2.

9 Conclusion

We propose a theoretically and empirically grounded, computationally efficient approach for fine-tuning diffusion models. This approach helps alleviate overoptimization issues and facilitates the generation of diverse samples. In future work, we plan to investigate the fine-tuning of recent diffusion models more tailored for biological or chemical applications (Watson et al., 2023; Avdeyev et al., 2023; Gruver et al., 2023).

Broader Impact

This paper presents work whose goal is to advance the field of machine learning. There are many potential societal consequences of our work, none of which we feel must be specifically highlighted here.

References

Avdeyev, P., C. Shi, Y. Tan, K. Dudnyk, and J. Zhou (2023). Dirichlet diffusion score model for biological sequence generation. *arXiv preprint arXiv:2305.10699*.

Bai, Y., S. Kadavath, S. Kundu, A. Askell, J. Kernion, A. Jones, A. Chen, A. Goldie, A. Mirhoseini, C. McKinnon, et al. (2022). Constitutional ai: Harmlessness from ai feedback. *arXiv preprint arXiv:2212.08073*.

Bansal, A., H.-M. Chu, A. Schwarzschild, S. Sengupta, M. Goldblum, J. Geiping, and T. Goldstein (2023). Universal guidance for diffusion models. In *Proceedings of the IEEE/CVF Conference on Computer Vision and Pattern Recognition*, pp. 843–852.

Barrera, L. A., A. Vedenko, J. V. Kurland, J. M. Rogers, S. S. Gisselbrecht, E. J. Rossin, J. Woodard, L. Mariani, K. H. Kock, S. Inukai, et al. (2016). Survey of variation in human transcription factors reveals prevalent dna binding changes. *Science* 351(6280), 1450–1454.

Berner, J., L. Richter, and K. Ullrich (2022). An optimal control perspective on diffusion-based generative modeling. *arXiv preprint arXiv:2211.01364*.

Bernton, E., J. Heng, A. Doucet, and P. E. Jacob (2019). Schrödinger bridge samplers. *arXiv preprint arXiv:1912.13170*.

Black, K., M. Janner, Y. Du, I. Kostrikov, and S. Levine (2023). Training diffusion models with reinforcement learning. *arXiv preprint arXiv:2305.13301*.

Casper, S., X. Davies, C. Shi, T. K. Gilbert, J. Scheurer, J. Rando, R. Freedman, T. Korbak, D. Lindner, P. Freire, et al. (2023). Open problems and fundamental limitations of reinforcement learning from human feedback. *arXiv preprint arXiv:2307.15217*.

Chen, R. T., Y. Rubanova, J. Bettencourt, and D. K. Duvenaud (2018). Neural ordinary differential equations. *Advances in neural information processing systems* 31.

Chen, T., B. Xu, C. Zhang, and C. Guestrin (2016). Training deep nets with sublinear memory cost. *arXiv preprint arXiv:1604.06174*.

Clark, K., P. Vicol, K. Swersky, and D. J. Fleet (2023). Directly fine-tuning diffusion models on differentiable rewards. *arXiv preprint arXiv:2309.17400*.

Cuturi, M. (2013). Sinkhorn distances: Lightspeed computation of optimal transport. *Advances in neural information processing systems* 26.

De Bortoli, V., J. Thornton, J. Heng, and A. Doucet (2021). Diffusion schrodinger bridge with applications to score-based generative modeling. *Advances in Neural Information Processing Systems* 34, 17695–17709.

Delbracio, M. and P. Milanfar (2023). Inversion by direct iteration: An alternative to denoising diffusion for image restoration. *arXiv preprint arXiv:2303.11435*.

Dhariwal, P. and A. Nichol (2021). Diffusion models beat gans on image synthesis. *Advances in neural information processing systems* 34, 8780–8794.

Fan, Y., O. Watkins, Y. Du, H. Liu, M. Ryu, C. Boutilier, P. Abbeel, M. Ghavamzadeh, K. Lee, and K. Lee (2023). Dpok: Reinforcement learning for fine-tuning text-to-image diffusion models. *arXiv preprint arXiv:2305.16381*.

Gao, L., J. Schulman, and J. Hilton (2023). Scaling laws for reward model overoptimization. In *International Conference on Machine Learning*, pp. 10835–10866. PMLR.

Ghari, P. M., A. Tseng, G. Eraslan, R. Lopez, T. Biancalani, G. Scalia, and E. Hajiramezanali (2023). Generative flow networks assisted biological sequence editing. In *NeurIPS 2023 Generative AI and Biology (GenBio) Workshop*.

Girolami, M. and B. Calderhead (2011). Riemann manifold langevin and hamiltonian monte carlo methods. *Journal of the Royal Statistical Society Series B: Statistical Methodology* 73(2), 123–214.

Graikos, A., N. Malkin, N. Jojic, and D. Samaras (2022). Diffusion models as plug-and-play priors. *Advances in Neural Information Processing Systems* 35, 14715–14728.

Gruslys, A., R. Munos, I. Danihelka, M. Lanctot, and A. Graves (2016). Memory-efficient backpropagation through time. *Advances in neural information processing systems* 29.

Gruver, N., S. Stanton, N. C. Frey, T. G. Rudner, I. Hotzel, J. Lafrance-Vanasse, A. Rajpal, K. Cho, and A. G. Wilson (2023). Protein design with guided discrete diffusion. *arXiv preprint arXiv:2305.20009*.

Heng, J., A. N. Bishop, G. Deligiannidis, and A. Doucet (2020). Controlled sequential monte carlo.

Ho, J., A. Jain, and P. Abbeel (2020). Denoising diffusion probabilistic models. *Advances in neural information processing systems* 33, 6840–6851.

Hu, E. J., Y. Shen, P. Wallis, Z. Allen-Zhu, Y. Li, S. Wang, L. Wang, and W. Chen (2021). Lora: Low-rank adaptation of large language models. *arXiv preprint arXiv:2106.09685*.

Jing, B., G. Corso, J. Chang, R. Barzilay, and T. Jaakkola (2022). Torsional diffusion for molecular conformer generation. *Advances in Neural Information Processing Systems* 35, 24240–24253.

Kappen, H. J. (2007). An introduction to stochastic control theory, path integrals and reinforcement learning. In *AIP conference proceedings*, Volume 887, pp. 149–181. American Institute of Physics.

Karatzas, I. and S. Shreve (2012). *Brownian motion and stochastic calculus*, Volume 113. Springer Science & Business Media.

Kidger, P., J. Foster, X. C. Li, and T. Lyons (2021). Efficient and accurate gradients for neural sdes. *Advances in Neural Information Processing Systems* 34, 18747–18761.

Lahlou, S., T. Deleu, P. Lemos, D. Zhang, A. Volokhova, A. Hernández-García, L. N. Ezzine, Y. Bengio, and N. Malkin (2023). A theory of continuous generative flow networks. In *International Conference on Machine Learning*, pp. 18269–18300. PMLR.

Lee, K., H. Liu, M. Ryu, O. Watkins, Y. Du, C. Boutilier, P. Abbeel, M. Ghavamzadeh, and S. S. Gu (2023). Aligning text-to-image models using human feedback. *arXiv preprint arXiv:2302.12192*.

Levine, S. (2018). Reinforcement learning and control as probabilistic inference: Tutorial and review. *arXiv preprint arXiv:1805.00909*.

Li, X., T.-K. L. Wong, R. T. Chen, and D. Duvenaud (2020). Scalable gradients for stochastic differential equations. In *International Conference on Artificial Intelligence and Statistics*, pp. 3870–3882. PMLR.

Lipman, Y., R. T. Chen, H. Ben-Hamu, M. Nickel, and M. Le (2023). Flow matching for generative modeling. *ICLR 2023*.

Liu, G.-H., A. Vahdat, D.-A. Huang, E. A. Theodorou, W. Nie, and A. Anandkumar (2023). I2sb: Image-to-image schrödinger bridge. *arXiv preprint arXiv:2302.05872*.

Loshchilov, I. and F. Hutter (2019). Decoupled weight decay regularization. In *International Conference on Learning Representations*.

Ma, Y.-A., Y. Chen, C. Jin, N. Flammarion, and M. I. Jordan (2019). Sampling can be faster than optimization. *Proceedings of the National Academy of Sciences* 116(42), 20881–20885.

Murray, N., L. Marchesotti, and F. Perronnin (2012). Ava: A large-scale database for aesthetic visual analysis. In *2012 IEEE conference on computer vision and pattern recognition*, pp. 2408–2415. IEEE.

Ouyang, L., J. Wu, X. Jiang, D. Almeida, C. Wainwright, P. Mishkin, C. Zhang, S. Agarwal, K. Slama, A. Ray, et al. (2022). Training language models to follow instructions with human feedback. *Advances in Neural Information Processing Systems 35*, 27730–27744.

Papamakarios, G., E. Nalisnick, D. J. Rezende, S. Mohamed, and B. Lakshminarayanan (2021). Normalizing flows for probabilistic modeling and inference. *The Journal of Machine Learning Research 22*(1), 2617–2680.

Prabhudesai, M., A. Goyal, D. Pathak, and K. Fragkiadaki (2023). Aligning text-to-image diffusion models with reward backpropagation. *arXiv preprint arXiv:2310.03739*.

Radford, A., J. W. Kim, C. Hallacy, A. Ramesh, G. Goh, S. Agarwal, G. Sastry, A. Askell, P. Mishkin, J. Clark, G. Krueger, and I. Sutskever (2021). Learning transferable visual models from natural language supervision. *arXiv preprint arXiv:2103.00020*.

Rombach, R., A. Blattmann, D. Lorenz, P. Esser, and B. Ommer (2022, June). High-resolution image synthesis with latent diffusion models. In *Proceedings of the IEEE/CVF Conference on Computer Vision and Pattern Recognition (CVPR)*, pp. 10684–10695.

Sarkisyan, K. S., D. A. Bolotin, M. V. Meer, D. R. Usmanova, A. S. Mishin, G. V. Sharonov, D. N. Ivankov, N. G. Bozhanova, M. S. Baranov, O. Soylemez, et al. (2016). Local fitness landscape of the green fluorescent protein. *Nature 533*(7603), 397–401.

Schrödinger, E. (1931). *Über die umkehrung der naturgesetze*. Verlag der Akademie der Wissenschaften in Kommission bei Walter De Gruyter u

Schuhmann, C. (2022, Aug). Laion aesthetics.

Schulman, J., F. Wolski, P. Dhariwal, A. Radford, and O. Klimov (2017). Proximal policy optimization algorithms. *arXiv preprint arXiv:1707.06347*.

Shi, Y., V. De Bortoli, A. Campbell, and A. Doucet (2023). Diffusion schr\” odinger bridge matching. *arXiv preprint arXiv:2303.16852*.

Shreve, S. E. et al. (2004). *Stochastic calculus for finance II: Continuous-time models*, Volume 11. Springer.

Sohl-Dickstein, J., E. Weiss, N. Maheswaranathan, and S. Ganguli (2015). Deep unsupervised learning using nonequilibrium thermodynamics. In *International conference on machine learning*, pp. 2256–2265. PMLR.

Somnath, V. R., M. Pariset, Y.-P. Hsieh, M. R. Martinez, A. Krause, and C. Bunne (2023). Aligned diffusion schr\” odinger bridges. *arXiv preprint arXiv:2302.11419*.

Song, J., C. Meng, and S. Ermon (2020). Denoising diffusion implicit models. *arXiv preprint arXiv:2010.02502*.

Song, Y., J. Sohl-Dickstein, D. P. Kingma, A. Kumar, S. Ermon, and B. Poole (2020). Score-based generative modeling through stochastic differential equations. *arXiv preprint arXiv:2011.13456*.

Stiennon, N., L. Ouyang, J. Wu, D. Ziegler, R. Lowe, C. Voss, A. Radford, D. Amodei, and P. F. Christiano (2020). Learning to summarize with human feedback. *Advances in Neural Information Processing Systems 33*, 3008–3021.

Theodorou, E., J. Buchli, and S. Schaal (2010). A generalized path integral control approach to reinforcement learning. *The Journal of Machine Learning Research 11*, 3137–3181.

Theodorou, E. A. and E. Todorov (2012). Relative entropy and free energy dualities: Connections to path integral and kl control. In *2012 ieee 51st ieee conference on decision and control (cdc)*, pp. 1466–1473. IEEE.

Tong, A., N. Malkin, G. Huguet, Y. Zhang, J. Rector-Brooks, K. Fatras, G. Wolf, and Y. Bengio (2023). Conditional flow matching: Simulation-free dynamic optimal transport. *arXiv preprint arXiv:2302.00482*.

Trabucco, B., X. Geng, A. Kumar, and S. Levine (2022). Design-bench: Benchmarks for data-driven offline model-based optimization. In *International Conference on Machine Learning*, pp. 21658–21676. PMLR.

Tzen, B. and M. Raginsky (2019). Theoretical guarantees for sampling and inference in generative models with latent diffusions. In *Conference on Learning Theory*, pp. 3084–3114. PMLR.

Wainwright, M. J. (2019). *High-dimensional statistics: A non-asymptotic viewpoint*, Volume 48. Cambridge university press.

Watson, D., W. Chan, J. Ho, and M. Norouzi (2022). Learning fast samplers for diffusion models by differentiating through sample quality. *arXiv preprint arXiv:2202.05830*.

Watson, J. L., D. Juergens, N. R. Bennett, B. L. Trippe, J. Yim, H. E. Eisenach, W. Ahern, A. J. Borst, R. J. Ragotte, L. F. Milles, et al. (2023). De novo design of protein structure and function with rfdiffusion. *Nature* 620(7976), 1089–1100.

Wu, L., C. Gong, X. Liu, M. Ye, and Q. Liu (2022). Diffusion-based molecule generation with informative prior bridges. *Advances in Neural Information Processing Systems* 35, 36533–36545.

Wu, X., K. Sun, F. Zhu, R. Zhao, and H. Li (2023). Better aligning text-to-image models with human preference. *arXiv preprint arXiv:2303.14420*.

Xu, J., X. Liu, Y. Wu, Y. Tong, Q. Li, M. Ding, J. Tang, and Y. Dong (2023). Imagereward: Learning and evaluating human preferences for text-to-image generation. *arXiv preprint arXiv:2304.05977*.

Yuan, H., K. Huang, C. Ni, M. Chen, and M. Wang (2023). Reward-directed conditional diffusion: Provable distribution estimation and reward improvement. In *Thirty-seventh Conference on Neural Information Processing Systems*.

Zhang, Q. and Y. Chen (2021). Path integral sampler: a stochastic control approach for sampling. *arXiv preprint arXiv:2111.15141*.

A Additional Related Works

In this section, we discuss additional related works.

Fine-tuning large language models. Much of the recent work in fine-tuning diffusion models is inspired by the wide success of fine-tuning large language models for various objectives such as instruction-following, summarization, or safety (Ouyang et al., 2022; Stiennon et al., 2020; Bai et al., 2022). Many techniques have been proposed to mitigate reward collapse in this domain, but KL regularization is the most commonly used (Gao et al., 2023). For a more comprehensive review, we direct readers to Casper et al. (2023). In our experiments, we compare to a KL-penalized RL baseline, which is analogous to the current dominant approach in language model fine-tuning.

Sampling and control. Control-based approaches have been extensively employed for generating samples from known unnormalized probability densities in various ways (Tzen and Raginsky, 2019; Bernton et al., 2019; Heng et al., 2020; Zhang and Chen, 2021; Berner et al., 2022; Lahliou et al., 2023). Notably, the most pertinent literature relates to path integral sampling (Zhang and Chen, 2021). Nevertheless, our work differs in terms of our target distribution and focus, which is primarily centered on fine-tuning. Additionally, their method often necessitates assuming the initial distribution to be a Dirac delta distribution, which is an assumption we cannot make. Our research also shares connections with path integral controls (Theodorou and Todorov, 2012; Theodorou et al., 2010; Kappen, 2007) and the concept of control as inference (Levine, 2018). However, our focus lies on the diffusion model, while their focus lies on standard RL problems.

Markov Chain Monte Carlo (MCMC). MCMC-based algorithms are commonly used for sampling from unnormalized densities that follow a proportionality of $\exp(r(x)/\alpha)$ (Girolami and Calderhead, 2011; Ma et al., 2019). Numerous MCMC methods have emerged, including the first-order technique referred to as MALA. The approach most closely related to incorporating MALA for fine-tuning is classifier-based guidance, as proposed in Dhariwal and Nichol (2021); Graikos et al. (2022). However, implementing classifier-based guidance is known to be unstable in practice due to the necessity of training numerous classifiers (Clark et al., 2023).

B Connection with Classifier Guidance

Recall the optimal SDE is written as

$$dx_t = \{f(t, x_t) + u^*(t, x_t)\}dt + \sigma(t)dw_t$$

where

$$u^*(t, x_t) = \sigma^2(t) \nabla_x \left\{ \log \mathbb{E}_{\mathbb{P}^{\text{data}}} \left[\exp \left(\frac{r(x_T)}{\alpha} \right) | x_t = x \right] \right\}.$$

When $r(x_T) = k(x_t) + \epsilon_t$ for some noise ϵ_t and a function $k : \mathbb{R}^d \rightarrow \mathbb{R}$, as we discuss in Section 7.1, the above is approximated as

$$u^*(t, x_t) = \frac{\sigma^2(t)}{\alpha} \nabla_x \mathbb{E}_{\mathbb{P}^{\text{data}}} [r(x_T) | x_t = x]. \quad (12)$$

Hence, at inference time, this boils down to using

$$dx_t = \left\{ f(t, x_t) + \frac{\sigma^2(t)}{\alpha} \nabla_{x_t} \mathbb{E}_{\mathbb{P}^{\text{data}}} [r(x_T) | x_t] \right\} + \sigma(t)dw_t.$$

This formulation has a close connection with classifier-based guidance. The naive adaptation of classifier guidance (Dhariwal and Nichol, 2021) in our context is

$$dx_t = \{f(t, x_t) + s'(t, x_t)\}dt + \sigma(t)dw_t$$

where

$$s'(t, x) = \nabla_x \log p(r(x_T) | x_t).$$

Supposing that $r(x_T) = k(x_t) + \epsilon$ where ϵ is a Gaussian noise with variance σ , this is equal to

$$\frac{1}{\sigma^2} \nabla_x \mathbb{E}_{\mathbb{P}^{\text{data}}} [r(x_T) | x_t = x].$$

Up to a constant, this takes the same form in (12).

C Proofs

C.1 Proof of Theorem 1

Let $\mathbb{P}_{\cdot|0}^u(\cdot|x_0)$ be the induced distribution by the SDE:

$$dx_t = \{f(t, x_t) + u(t, x_t)\}dt + \sigma(t)dw_t.$$

over \mathcal{C} conditioning on x_0 . Similarly, let $\mathbb{P}_{\cdot|0}^{\text{data}}(\cdot|x_0)$ be the induced distribution by the SDE:

$$dx_t = f(t, x_t)dt + \sigma(t)dw_t$$

over \mathcal{C} conditioning on x_0 .

Now, we calculate the KL divergence of $\mathbb{P}_{\cdot|0}^{\text{data}}(\cdot|x_0)$ and $\mathbb{P}_{\cdot|0}^u(\cdot|x_0)$. This is equal to

$$\text{KL}(\mathbb{P}_{\cdot|0}^u(\cdot|x_0) \parallel \mathbb{P}_{\cdot|0}^{\text{data}}(\cdot|x_0)) = \mathbb{E}_{\{x_t\} \sim \mathbb{P}_{\cdot|0}^u(\cdot|x_0)} \left[\int_0^T \frac{1}{2} \frac{\|u(t, x_t)\|^2}{\sigma^2(t)} dt \right]. \quad (13)$$

This is because

$$\begin{aligned} \text{KL}(\mathbb{P}_{\cdot|0}^u(\cdot|x_0) \parallel \mathbb{P}_{\cdot|0}^{\text{data}}(\cdot|x_0)) &= \mathbb{E}_{\mathbb{P}_{\cdot|0}^u(\cdot|x_0)} \left[\frac{d\mathbb{P}_{\cdot|0}^u(\cdot|x_0)}{d\mathbb{P}_{\cdot|0}^{\text{data}}(\cdot|x_0)} \right] \\ &= \mathbb{E}_{\mathbb{P}_{\cdot|0}^u(\cdot|x_0)} \left[\int_0^T \frac{1}{2} \frac{\|u(t, x_t)\|^2}{\sigma^2(t)} dt + \int_0^T u(t, x_t)dw_t \right] \\ &\quad \text{(Girsanov theorem)} \\ &= \mathbb{E}_{\mathbb{P}_{\cdot|0}^u(\cdot|x_0)} \left[\int_0^T \frac{1}{2} \frac{\|u(t, x_t)\|^2}{\sigma^2(t)} dt \right]. \\ &\quad \text{(Martingale property of Itô integral)} \end{aligned}$$

Therefore, the objective function in (5) is equivalent to

$$\text{obj} = \mathbb{E}_{\mathbb{P}^{u,\nu}}[r(x_T)] - \alpha \text{KL}(\mathbb{P}^{u,\nu} \parallel \mathbb{P}^{\text{data}}). \quad (14)$$

This is because

$$\begin{aligned} \mathbb{E}_{\mathbb{P}^{u,\nu}}[r(x_T)] - \alpha \text{KL}(\nu \parallel \nu_{\text{ini}}) - \alpha \mathbb{E}_{\mathbb{P}^{u,\nu}} \left[\int_0^T \frac{1}{2} \frac{\|u(t, x_t)\|^2}{\sigma^2(t)} dt \right] \\ = \mathbb{E}_{\mathbb{P}^{u,\nu}}[r(x_T)] - \alpha \text{KL}(\nu \parallel \nu_{\text{ini}}) - \alpha \mathbb{E}_{x_0 \sim \nu} \left[\text{KL}(\mathbb{P}_{\cdot|0}^u(\cdot|x_0) \parallel \mathbb{P}_{\cdot|0}^{\text{data}}(\cdot|x_0)) \right] \\ = \mathbb{E}_{\mathbb{P}^{u,\nu}}[r(x_T)] - \alpha \text{KL}(\mathbb{P}^{u,\nu} \parallel \mathbb{P}^{\text{data}}). \end{aligned}$$

The objective function is further changed as follows:

$$\begin{aligned} \text{obj} &= \mathbb{E}_{\mathbb{P}^{u,\nu}}[r(x_T)] - \alpha \text{KL}(\mathbb{P}^{u,\nu} \parallel \mathbb{P}^{\text{data}}) \\ &= \underbrace{\mathbb{E}_{x_T \sim \mathbb{P}_T^u}[r(x_T)] - \alpha \text{KL}(\mathbb{P}_T^{u,\nu} \parallel \mathbb{P}_T^{\text{data}})}_{\text{Term (a)}} - \underbrace{\alpha \mathbb{E}_{x_T \sim \mathbb{P}_T^u} [\text{KL}(\mathbb{P}_T^{u,\nu}(\tau|x_T) \parallel \mathbb{P}_T^{\text{data}}(\tau|x_T))]}_{\text{Term (b)}}. \end{aligned}$$

By optimizing (a) and (b) over $\mathbb{P}^{u,\nu}$, we get

$$\begin{aligned} \mathbb{P}_T^*(x_T) &= \exp(r(x_T)/\alpha) \mathbb{P}^{\text{data}}(x_T)/C, \\ \mathbb{P}_T^*(\tau|x_T) &= \mathbb{P}_T^{\text{data}}(\tau|x_T). \end{aligned} \quad (15)$$

Hence, we have

$$\mathbb{P}^*(\tau) = \mathbb{P}_T^*(x_T) \times \mathbb{P}_T^*(\tau|x_T) = \frac{\exp(r(x_T)/\alpha) \mathbb{P}^{\text{data}}(\tau)}{C}.$$

Remark 2. Some readers might wonder, since we originally optimized over u, ν but not $\mathbb{P}^{u,\nu}$, the last step might be sloppy. We chose this proof first because this proof can more clearly convey our message of bridge preserving property in (15). We will formalize it in Section C.2.

Marginal distribution at t . Finally, consider the marginal distribution at t . By marginalizing before t , we get

$$\mathbb{P}_{[t,T]}^{\text{data}}(\tau_{[t,T]}) \times \exp(r(x_T)/\alpha)/C.$$

Next, by marginalizing after t ,

$$\mathbb{P}_t^{\text{data}}(x)/C \times \mathbb{E}_{\mathbb{P}_{\text{data}}}[\exp(r(x_T)/\alpha)|x_t = x].$$

Using Feynman–Kac formulation in Lemma 1, this is equivalent to

$$\mathbb{P}_t^{\text{data}}(x) \exp(v_t^*(x)/\alpha)/C.$$

Marginal distribution at T . We marginalize before T . We have the following

$$\mathbb{P}_T^{\text{data}}(x) \exp(r(x)/\alpha)/C.$$

C.2 Another Proof of Theorem 1

First, noting the loss in (5) becomes

$$\mathbb{E}_{x_0 \sim \nu}[v_0^*(x_0) - \alpha \text{KL}(\nu(x_0)/\nu_{\text{ini}}(x_0))],$$

by optimizing over $\nu \in \Delta(\mathcal{X})$, we can easily prove that the optimal initial distribution is

$$\exp\left(\frac{v_0^*(x)}{\alpha}\right) \nu_{\text{ini}}(x)/C.$$

Hereafter, our goal is to prove that the marginal distribution at t (i.e., \mathbb{P}_t^*) is indeed $q_t(x)$ defined by

$$g_t(x) := \exp\left(\frac{v_t^*(x)}{\alpha}\right) \mathbb{P}_t^{\text{data}}(x)/C$$

Recall we have seen that the SDE with the optimal drift term is

$$dx_t = \left\{ f(t, x) + \frac{\sigma^2(t)}{\alpha} \nabla v_t^*(x) \right\} dt + \sigma(t) dw_t.$$

Then, what we need to prove is that the density $g_t(x)$ satisfies the Kolmogorov forward equation:

$$\frac{dg_t(x)}{dt} + \sum_i \frac{d}{dx^{[i]}} \left[\left\{ f^{[i]}(t, x) + \frac{\sigma^2(t)}{\alpha} \nabla_{x^{[i]}} v_t^*(x) \right\} g_t(x) \right] - \frac{\sigma^2(t)}{2} \sum_i \frac{d^2 g_t(x)}{dx^{[i]} dx^{[i]}} = 0. \quad (16)$$

where $f = [f^{[1]}, \dots, f^{[d]}]^\top$ and Indeed, it is proved as follows.

$$\begin{aligned} & \frac{dg_t(x)}{dt} + \sum_i \frac{d}{dx^{[i]}} \left[\left\{ f^{[i]}(t, x) + \frac{\sigma^2(t)}{\alpha} \nabla_{x^{[i]}} v_t^*(x) \right\} g_t(x) \right] - \frac{\sigma^2(t)}{2} \sum_i \frac{d^2 g_t(x)}{dx^{[i]} dx^{[i]}} \\ &= \frac{1}{C} \exp\left(\frac{v_t^*(x)}{\alpha}\right) \left\{ \frac{d\mathbb{P}_t^{\text{data}}(x)}{dt} + \sum_i \nabla_{x^{[i]}} (\mathbb{P}_t^{\text{data}}(x) f^{[i]}(t, x)) - \frac{\sigma^2(t)}{2} \sum_i \frac{d^2 \mathbb{P}_t^{\text{data}}(x)}{dx^{[i]} dx^{[i]}} \right\} \\ &+ \frac{1}{C} \mathbb{P}_t^{\text{data}}(x) \left\{ \frac{d \exp(v_t^*(x)/\alpha)}{dt} + \sum_i f^{[i]}(t, x) \nabla_{x^{[i]}} (\exp(v_t^*(x)/\alpha)) - \frac{\sigma^2(t)}{2} \sum_i \frac{d^2 \exp(v_t^*(x)/\alpha)}{dx^{[i]} dx^{[i]}} \right\} \\ &+ \frac{1}{C} \mathbb{P}_t^{\text{data}}(x) \times \frac{\sigma^2(t)}{2} \sum_i \frac{d^2 \exp(v_t^*(x)/\alpha)}{dx^{[i]} dx^{[i]}}. \end{aligned}$$

Hence, the above is equal to 0 since, from the Kolmogorov forward equation, we have

$$\frac{d\mathbb{P}_t^{\text{data}}(x)}{dt} + \sum_i \nabla_{x^{[i]}} (\mathbb{P}_t^{\text{data}}(x) f^{[i]}(t, x)) - \frac{\sigma^2(t)}{2} \sum_i \frac{d^2 \mathbb{P}_t^{\text{data}}(x)}{dx^{[i]} dx^{[i]}} = 0,$$

and the optimal value function satisfies the following

$$\frac{\sigma^2(t)}{2} \sum_i \frac{d^2 \exp(v_t^*(x)/\alpha)}{dx^{[i]} dx^{[i]}} + f \cdot \nabla \exp(v_t^*(x)/\alpha) + \frac{d \exp(v_t^*(x)/\alpha)}{dt} = 0,$$

which will be shown in the proof of Lemma 1 as in (19). Hence, (16) is proved, and q_t is \mathbb{P}_t^* .

C.3 Proof of Lemma 1

From the Hamilton–Jacobi–Bellman (HJB) equation, we have

$$\max_u \left\{ \frac{\sigma^2(t)}{2} \sum_i \frac{d^2 v_t^*(x)}{dx^{[i]} dx^{[i]}} + \{f + u\} \cdot \nabla v_t^*(x) + \frac{dv_t^*(x)}{dt} - \frac{\alpha \|u\|_2^2}{2\sigma^2(t)} \right\} = 0. \quad (17)$$

where $x^{[i]}$ is a i -th element in x . Hence, by simple algebra, we can prove that the optimal control satisfies

$$u^*(t, x) = \frac{\sigma^2(t)}{\alpha} \nabla v_t^*(x).$$

By plugging the above into the HJB equation (17), we get

$$\frac{\sigma^2(t)}{2} \sum_i \frac{d^2 v_t^*(x)}{dx^{[i]} dx^{[i]}} + f \cdot \nabla v_t^*(x) + \frac{dv_t^*(x)}{dt} + \frac{\sigma^2(t) \|\nabla v_t^*(x)\|_2^2}{2\alpha} = 0, \quad (18)$$

which characterizes the optimal value function. Now, using (18), we can show

$$\begin{aligned} & \frac{\sigma^2(t)}{2} \sum_i \frac{d^2 \exp(v_t^*(x)/\alpha)}{dx^{[i]} dx^{[i]}} + f \cdot \nabla \exp(v_t^*(x)/\alpha) + \frac{d \exp(v_t^*(x)/\alpha)}{dt} \\ &= \exp\left(\frac{v_t^*(x)}{\alpha}\right) \times \left\{ \frac{\sigma^2(t)}{2} \sum_i \frac{d^2 v_t^*(x)}{dx^{[i]} dx^{[i]}} + f \cdot \nabla v_t^*(x) + \frac{dv_t^*(x)}{dt} + \frac{\sigma^2(t) \|\nabla v_t^*(x)\|_2^2}{2\alpha} \right\} \\ &= 0. \end{aligned}$$

Therefore, to summarize, we have

$$\frac{\sigma^2(t)}{2} \sum_i \frac{d^2 \exp(v_t^*(x)/\alpha)}{dx^{[i]} dx^{[i]}} + f \cdot \nabla \exp(v_t^*(x)/\alpha) + \frac{d \exp(v_t^*(x)/\alpha)}{dt} = 0, \quad (19)$$

$$v_T^*(x) = r(x). \quad (20)$$

Finally, by invoking the Feynman–Kac formula (Shreve et al., 2004), we obtain the conclusion:

$$\exp\left(\frac{v_t^*(x)}{\alpha}\right) = \mathbb{E}_{\mathbb{P}^{\text{data}}} \left[\exp\left(\frac{r(x_T)}{\alpha}\right) | x_t = x \right].$$

C.4 Proof of Lemma 2

Recall $u^*(t, x) = \frac{\sigma^2(t)}{\alpha} \times \nabla_x v_t^*(x)$ from the proof of Lemma 1. Then, we have

$$\begin{aligned} u^*(t, x) &= \frac{\sigma^2(t)}{\alpha} \times \nabla_x v_t^*(x) = \frac{\sigma^2(t)}{\alpha} \times \alpha \frac{\nabla_x \exp(v_t^*(x)/\alpha)}{\exp(v_t^*(x)/\alpha)} \\ &= \sigma^2(t) \times \frac{\nabla_x \mathbb{E}_{\mathbb{P}^{\text{data}}} [\exp(r(x_T)/\alpha) | x_t = x]}{\mathbb{E}_{\mathbb{P}^{\text{data}}} [\exp(r(x_T)/\alpha) | x_t = x]}. \end{aligned}$$

C.5 Proof of Lemma 3

Recall

$$\mathbb{P}^*(\tau) = \mathbb{P}^{\text{data}}(\tau) \exp(r(x_T)/\alpha)/C$$

By marginalizing before s , we get

$$\mathbb{P}_{[s, T]}^*(\tau_{[s, T]}) \times \exp(r(x_T)/\alpha)/C$$

Next, marginalizing after t ,

$$\begin{aligned} & \mathbb{P}_{[s, t]}^*(\tau_{[s, t]}) \times \mathbb{E}_{\mathbb{P}^{\text{data}}} [\exp(r(x_T)/\alpha) | x_t] / C \\ &= \mathbb{P}_{[s, t]}^*(\tau_{[s, t]}) \exp(v_t^*(x_t)/\alpha) / C. \end{aligned}$$

Finally, by marginalizing between s and t , the joint distribution at (s, t) is

$$\mathbb{P}_{s, t}^{\text{data}}(x_s, x_t) \exp(v_t^*(x_t)/\alpha) / C.$$

Forward conditional distribution.

$$\mathbb{P}_{t|s}^*(x_t|x_s) = \frac{\mathbb{P}_{s,t}^{\text{data}}(x_s, x_t) \exp(v_t^*(x_t)/\alpha)/C}{\mathbb{P}_s^{\text{data}}(x_s) \exp(v_s^*(x_s)/\alpha)/C} = \mathbb{P}_{s|t}^{\text{data}}(x_t|x_s) \frac{\exp(v_t^*(x_t)/\alpha)}{\exp(v_s^*(x_s)/\alpha)}.$$

Backward conditional distribution.

$$\mathbb{P}_{s|t}^*(x_s|x_t) = \frac{\mathbb{P}_{s,t}^{\text{data}}(x_s, x_t) \exp(v_t^*(x_t)/\alpha)/C}{\mathbb{P}_s^{\text{data}}(x_t) \exp(v_t^*(x_t)/\alpha)/C} = \mathbb{P}_{s|t}^{\text{data}}(x_s|x_t).$$

C.6 Proof of Lemma 4

Use a statement in (15) the proof of Theorem 1.

C.7 Proof of Theorem 2

We omit the proof since it is the same as the proof of Theorem 1.

D Diffusion models

In this section, we provide an overview of continuous-time generative models. The objective is to train a SDE in such a way that the marginal distribution at time T follows p_{data} . While p_{data} is not known, we do have access to a dataset that follows this distribution.

Denoising diffusion models DDPMs (Song et al., 2020) are a widely adopted class of generative models. We start by considering a forward stochastic differential equation (SDE) represented as:

$$d\mathbf{y}_t = -0.5\mathbf{y}_t dt + dw_t, \mathbf{y}_0 \sim p_{\text{data}}, \quad (21)$$

defined on the time interval $[0, T]$. As T tends toward infinity, the limit of this distribution converges to $\mathcal{N}(0, \mathbb{I}_d)$, where \mathbb{I}_d denotes a d -dimensional identity matrix. Let \mathbb{Q} be a measure on \mathcal{C} induced by the forward SDE (21). Consequently, a generative model can be defined using its time-reversal: $x_t = \mathbf{y}_{T-t}$, which is characterized by:

$$dx_t = \{0.5x_t - \nabla \log \mathbb{Q}_{T-t}(x_t)\}dt + dw_t, x_0 \sim \mathcal{N}(0, \mathbb{I}_d).$$

A core aspect of DDPMs involves learning the score $\nabla \log \mathbb{Q}_t$ by optimizing the following loss with respect to S :

$$\mathbb{E}_{\mathbb{Q}}[\|\nabla \log \mathbb{Q}_{t|0}(x_t|x_0) - S(t, x_t)\|_2^2].$$

A potential limitation of the above approach is that the forward SDE (21) might not converge to a predefined prior distribution, such as $\mathcal{N}(0, \mathbb{I}_d)$, within a finite time T . To address this concern, we can employ the Schrödinger Bridge formulation (De Bortoli et al., 2021).

Diffusion Schrödinger Bridge. A potential bottleneck of the diffusion model is that the forward SDE might not converge to a pre-specified prior $\mathcal{N}(0, \mathbb{I}_d)$ with finite T . To mitigate this problem, De Bortoli et al. (2021) proposed the following Diffusion Schrödinger Bridge. Being inspired by Schrödinger Bridge formulation (Schrödinger, 1931) they formulate the problem:

$$\underset{\mathbb{P}}{\text{argmin}} \text{KL}(\mathbb{P} \parallel \mathbb{P}_{\text{ref}}) \text{ s.t. } \mathbb{P}_0 = \nu_{\text{ini}}, \mathbb{P}_T = p_{\text{data}}.$$

where \mathbb{P}_{ref} is a reference distribution on \mathcal{C} such as a Wiener process, \mathbb{P}_0 is a margin distribution of \mathbb{P} at time 0, and \mathbb{P}_T is similarly defined. To solve this problem, De Bortoli et al. (2021) proposed an iterative proportional fitting, which is a continuous extension of the Sinkhorn algorithm (Cuturi, 2013), while learning the score functions from the data as in DDM.

Bridge Matching. In DDPMs, we have formulated a generative model based on the time-reversal process and aimed to learn a score function $\nabla \log \mathbb{Q}_t$ from the data. Another recent popular approach involves emulating the reference Brownian bridge given $0, T$ with fixed a pre-defined initial distribution ν_{ini} and a data distribution p_{data} at time T (Shi et al., 2023). To elaborate further, let's begin by introducing a reference SDE:

$$d\bar{x}_t = \sigma(t)dw_t, \quad \bar{x}_0 \sim \nu_{\text{ini}}.$$

Here, we overload the notation with \mathbb{Q} to indicate an induced SDE. The Brownian bridge $\mathbb{Q}_{\cdot|[0,T]}(\cdot|x_0, x_T)$ is defined as:

$$d\bar{x}_t^{0,T} = \sigma(t)^2 \nabla \log \mathbb{Q}_{T|t}(x_T|\bar{x}_t^{0,T}) + \sigma(t)dw_t, x_0^{0,T} = x_0,$$

where $x_T^{0,T} = x_T$. The explicit calculation of this Brownian bridge is given by:

$$\nabla \log \mathbb{Q}_{T|t}(x_T|\bar{x}_t^{0,T}) = \frac{x_T - x_t}{T - t} dt + \sigma(t)w_t.$$

Now, we define a target SDE as follows:

$$dx_t = f(t, x_t)dt + \sigma(t)dw_t, \quad x_0 \sim \nu_{\text{ini}}.$$

This SDE aims to induce the same Brownian bridge as described earlier and should generate the distribution p_{data} at time T . We use \mathbb{P} to denote the measure induced by this SDE. While the specific drift term f is unknown, we can sample any time point t ($0 < t < T$) from \mathbb{P} by first sampling x_0 and x_T from ν_{ini} and p_{data} , respectively, and then sampling from the reference bridge, i.e., the Brownian bridge. To learn this drift term f , we can use the following characterization:

$$f(t, x_t) = \mathbb{E}_{\mathbb{P}}[\nabla \log \mathbb{Q}_{T|t}(x_T|x_t)|x_t = x_t].$$

Subsequently, the desired drift term can be learned using the following loss function with respect to f :

$$\mathbb{E}_{\mathbb{P}}[\|\nabla \log \mathbb{Q}_{T|t}(x_T|x_t) - f(t, x_t)\|^2].$$

Bridge matching can be formulated in various equivalent ways, and for additional details, we refer the readers to Shi et al. (2023).

E Details of Implementation

E.1 Implementation Details of Neural SDE

We aim to solve

$$\underset{\bar{f}: [0, T] \times \mathcal{Z} \rightarrow \mathcal{Z}}{\text{argmax}} \quad L(z_T), dz_t = \bar{f}(t, z_t)dt + \bar{g}(t)dw_t, z_0 \sim \bar{\nu}.$$

Here is a simple method we use. Regarding more details, refer to Kidger et al. (2021); Chen et al. (2018).

Suppose \bar{f} is parametrized by θ . Then, we update this θ with SGD. Consider at iteration j . Fix θ_j in $\bar{f}(t, z_t; \theta_j)$. By simulating an SDE with

$$dz_t = \bar{f}(t, z_t; \theta_j)dt + \bar{g}(t)dw_t, z_0 \sim \bar{\nu},$$

we obtain n trajectories

$$\{z_0^{(i)}, \dots, z_T^{(i)}\}_{i=1}^n.$$

In this step, we are able to use any off-the-shelf discretization methods. For example, starting from $z_0^{(i)} \sim \nu$, we are able to obtain a trajectory as follows:

$$z_t^{(i)} = z_{t-1}^{(i)} + \bar{f}(t-1, z_{t-1}^{(i)}; \theta_j)\Delta t + \bar{g}(t-1)\Delta w_t, \quad \Delta w_t \sim \mathcal{N}(0, (\Delta t)^2).$$

Finally, we update θ with the following:

$$\theta_{j+1} = \theta_j + \alpha \nabla_{\theta} \left\{ \frac{1}{n} \sum_{i=1}^n (L(z_T^{(i)})) \right\} \Big|_{\theta=\theta_j}.$$

We use Adam in this step for the practical selection of α .

E.2 More Refined Methods to Learn Value Functions

We can directly get a pair of x and y . Here, $\{x^{(i)}\} \sim \nu_{\text{ini}}$ and

$$\hat{y}^{(i)} := \alpha \log \hat{\mathbb{E}}_{\mathbb{P}^{\text{data}}} [\exp(r(x_T)/\alpha) | x_0 = x^{(i)}]$$

where $\hat{\cdot}$ means Monte Carlo approximation for each x_i . In other words,

$$\hat{\mathbb{E}}_{\mathbb{P}^{\text{data}}} [\exp(r(x_T)/\alpha) | x_0 = x_i] := \frac{1}{n} \sum_{j=1}^n \exp(r(x_T^{(i,j)})/\alpha)$$

where $\{r(x_T^{(i,j)})\}$ is a set of samples following \mathbb{P}^{data} with initial condition: $x_0 = x_i$. Then, we are able to learn a using the following ERM:

$$\hat{a} = \operatorname{argmin}_{a \in \mathcal{A}} \sum_{i=1}^n \{a(x^{(i)}) - \hat{y}^{(i)}\}^2.$$

E.3 Baselines

We consider the following baselines.

PPO + KL. Considering the discretized formulation of diffusion models (Black et al., 2023; Fan et al., 2023), we use the following update rule:

$$\nabla_{\theta} \mathbb{E}_{\mathcal{D}} \sum_{t=1}^T \left[\min \left\{ \tilde{r}_t(x_0, x_t) \frac{p(x_t | x_{t-1}; \theta)}{p(x_t | x_{t-1}; \theta_{\text{old}})}, \tilde{r}_t(x_0, x_t) \cdot \text{Clip} \left(\frac{p(x_t | x_{t-1}; \theta)}{p(x_t | x_{t-1}; \theta_{\text{old}})}, 1 - \epsilon, 1 + \epsilon \right) \right\} \right], \quad (22)$$

$$\tilde{r}_t(x_0, x_t) = -r(x_T) + \underbrace{\alpha \frac{\|u(t, x_t; \theta)\|^2}{2\sigma^2(t)}}_{\text{KL term}}, \quad p(x_t | x_{t-1}; \theta) = \mathcal{N}(u(t, x_t; \theta) + f(t, x_t), \sigma(t)) \quad (23)$$

where $f(t, x_t)$ is a pre-trained drift term and θ is a parameter to optimize.

Note that DPOK (Fan et al., 2023) uses the following update:

$$\nabla_{\theta} \mathbb{E}_{\mathcal{D}} \sum_{t=1}^T \left[\min \left\{ -r(x_0) \frac{p(x_t | x_{t-1}; \theta)}{p(x_t | x_{t-1}; \theta_{\text{old}})}, -r(x_0) \cdot \text{Clip} \left(\frac{p(x_t | x_{t-1}; \theta)}{p(x_t | x_{t-1}; \theta_{\text{old}})}, 1 - \epsilon, 1 + \epsilon \right) \right\} + \underbrace{\alpha \frac{\|u(t, x_t; \theta)\|^2}{2\sigma^2(t)}}_{\text{KL term}} \right]$$

where the KL term is directly differentiated. We did not use the DPOK update rule because DDPO appears to outperform DPOK even without a KL penalty (Black et al. (2023), Appendix C), so we implemented this baseline by modifying the DDPO codebase to include the added KL penalty term (Equation (23)).

Guidance. We use the following implementation of guidance (Dhariwal and Nichol, 2021):

- For each $t \in [0, T]$, we train a model: $\mathbb{P}_t(y | x_t)$ where x_t is a random variable induced by the pre-trained diffusion model.
- We fix a guidance level $\gamma \in \mathbb{R}_{>0}$, target value $y_{\text{con}} \in \mathbb{R}$, and at inference time (during each sampling step), we use the following score function

$$\nabla_x \log \mathbb{P}_t(y = y_{\text{con}} | x) = \nabla_x \log \mathbb{P}_t(x) + \gamma \nabla_x \log \mathbb{P}_t(y = y_{\text{con}} | x).$$

A remaining question is how to model $p(y | x)$. In our case, for the biological example, we make a label depending on whether x is top 10% or not and train a binary classifier. In image experiments, we construct a Gaussian model: $p(y | x) = \mathcal{N}(y - \mu_{\theta}(x), \sigma^2)$ where y is the reward label, μ_{θ} is the reward model we need to train, and σ is a fixed hyperparameter.

Table 4: Architecture of diffusion models for TFBind

Layer	Input Dimension	Output dimension	Explanation
1	1 (t)	256 (t')	Get time feature
1	$8 \times 4 (x)$	64 (x')	Get positional encoder (Denote x')
2	$8 \times 4 + 256 + 64 (x, t, x')$	64 (\bar{x})	Transformer encoder
3	64 (\bar{x})	$8 \times 4 (x)$	Linear

Table 5: Architecture of oracles for TFBind

	Input dimension	Output dimension	Explanation
1	8×4	500	Linear
1	500	500	ReLU
2	500	200	Linear
2	200	200	ReLU
3	200	1	Linear
3	200	1	ReLU
4	1	1	Sigmoid

F Experiment Details

F.1 Details for Tasks in Biological Sequences

F.1.1 Dataset.

TFBind8. The number of original dataset size is 65792. Each data consists of a DNA sequence with 8-length. We represent each data as a one-hot encoding vector with dimension 8×4 . To construct diffusion models, we use all datasets. We use half of the dataset to construct a learned reward r to make a scenario where oracles are imperfect.

GFP. The original dataset contains 56,086 data points, each comprising an amino acid sequence with a length of 237. We represent each data point using one-hot encoding with a dimension of 237×20 . Specifically, we model the difference between the original sequence and the baseline sequence. For our experiments, we selected the top 33,637 samples following (Trabucco et al., 2022) and trained diffusion models and oracles using this selected dataset.

F.1.2 Structure of Neural Networks.

We describe the implementation of neural networks in more detail.

Diffusion models and fine-tuning. For diffusion models in TFBind, we use a neural network to model score functions in Table 4. We use a similar network for the GFP dataset and fine-tuning parts.

Oracles to obtain score functions. To construct oracles in TFBind, we employ the neural networks listed in Table 5. For GFP, we utilize a similar network.

F.1.3 Hyperparameters

We report a set of important hyperparameters in Table 6.

F.1.4 Additional Results

We add the enlarged figure of **ELEGANT** (0.005) in Table 2.

F.2 Details for Image Tasks

Below, we explain the training details and list hyperparameters in Table 7.

Table 6: Primary hyperparameters for fine-tuning. For all methods, we use the Adam optimizer.

Method	Type	GFP	TFBind
ELEGANT	Batch size	128	128
	Sampling for neural SDE	Euler Maruyama	
	Step size (fine-tuning)	50	50
	Epochs (fine-tuning)	50	50
PPO	Batch size	128	128
	ϵ	0.1	0.1
	Epochs	100	100
Guidance	Guidance level	30	30
Pre-trained diffusion	Forward SDE	Variance preserving	
	Sampling way	Euler Maruyama	

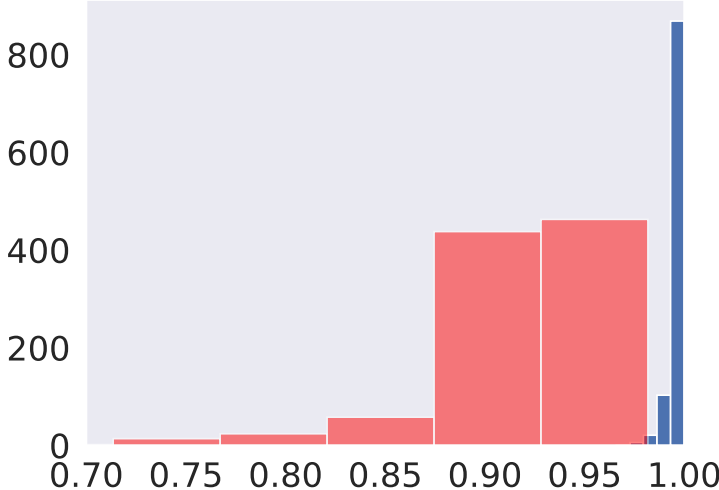


Figure 5: Enlarge histogram of **ELEGANT** (0.005) in Table 2.

F.2.1 Details of Implementation

We use 4 A100 GPUs for all the image tasks. We use the AdamW optimizer (Loshchilov and Hutter, 2019) with $\beta_1 = 0.9$, $\beta_2 = 0.999$ and weight decay of 0.1. To ensure consistency with previous research, in fine-tuning, we also employ training prompts that are uniformly sampled from 50 common animals (Black et al., 2023; Prabhudesai et al., 2023).

Sampling. We use the DDIM sampler with 50 diffusion steps (Song et al., 2020). Since we need to back-propagate the gradient of rewards through both the sampling process producing the latent representation and the VAE decoder used to obtain the image, memory becomes a bottleneck. We employ two designs to alleviate memory usage following Clark et al. (2023); Prabhudesai et al. (2023): (1) Fine-tuning low-rank adapter (LoRA) modules (Hu et al., 2021) instead of tuning the original diffusion weights, and (2) Gradient checkpointing for computing partial derivatives on demand (Gruslys et al., 2016; Chen et al., 2016). The two designs make it possible to back-propagate gradients through all 50 diffusing steps in terms of hardware.

Guidance. To train the classifier, we use the AVA dataset (Murray et al., 2012) which includes more than 250k evaluations (i.e., 20 times more samples than our **ELEGANT** implementation, cf. Figure 3). We implement the classifier (i.e., reward model) using an MLP model that takes the concatenation of sinusoidal time embeddings (for time t) and CLIP embeddings (Radford et al., 2021) (for x_t) as input. The implementation is based on the public RCGDM (Yuan et al., 2023) codebase⁴.

⁴<https://github.com/Kaffaljidhmah2/RCGDM>

Table 7: Training hyperparameters.

Hyperparameter	
Learning rate	1e-4
Batch size per GPU	4
Clip grad norm	5.0
DDIM steps	50
Guidance weight	7.5
Samples per iteration	128

Table 8: Results for aesthetic scores. We set $\alpha = 1$ for **ELEGANT** and set $\alpha = 0.001$ for **PPO + KL**. (·) are confidence intervals.

	Reward (r) \uparrow	KL-Div \downarrow
NO KL	8.80 ± 0.08	6.03
Guidance	6.41 ± 0.19	5.99
PPO + KL	5.98 ± 0.35	0.03
ELEGANT (Ours)	8.62 ± 0.16	0.34

F.2.2 Additional Results

In Table 8, we report the performances of our **ELEGANT** and baselines in fine-tuning aesthetic scores. We provide more qualitative samples to illustrate the performances in Figure 7. From the visual evidence, **ELEGANT** with $\alpha = 10$ consistently produces images with higher scores compared to the baseline, suggesting an improved capacity for generating high-fidelity images. This improvement is maintained, albeit to a slightly lesser degree, even when the α parameter is reduced to 1.

Compared with NO KL. Qualitatively, the images generated by **ELEGANT** are depicted with a high level of detail and realism, which may be indicative of the algorithm’s capability to preserve the distinctive features of each species. The **NO KL** baseline falls short in achieving scores comparable to those of **ELEGANT**, particularly notable in the representations of the hippopotamus and the crocodile. Moreover, experimentally we observe severe reward collapse as early as the 10th epoch of **NO KL** (at the time, the reward is ≈ 7), which indicates that even if the optimization continues (i.e., reward score rises), it is meaningless because **NO KL** fails to produce meaningful generations afterward. Reward collapse is regarded as a major issue in reward-guided diffusion model fine-tuning (Clark et al., 2023; Prabhudesai et al., 2023).

Compared with Guidance. In practice, we observe that the guidance strength in **Guidance** is hard to control: if the guidance level and target level are not strong, the reward-guided generation would be weak (cf. Table 9). However, with a strong guidance signal and a high target value, the generated images become more colorful at the expense of degradation of the image qualities. In presenting qualitative results in Figure 7, we set the target as 10 and the guidance level as 200 to balance generation performance and fidelity.

Compared with PPO. We plot the training curves of **PPO**, **PPO + KL**, versus **ELEGANT** in Figure 6. Empirically, we observe **PPO** outperforms **PPO + KL** in terms of reward but still falls short compared to our **ELEGANT**.

Compared with PPO + KL. As a KL-regularized PPO-based algorithm, **PPO + KL** maintains a stable generation quality and is robust in KL divergence, indicating a stable optimization process. However, with limited training samples, this baseline becomes inefficient in both training time and synthesis performances.

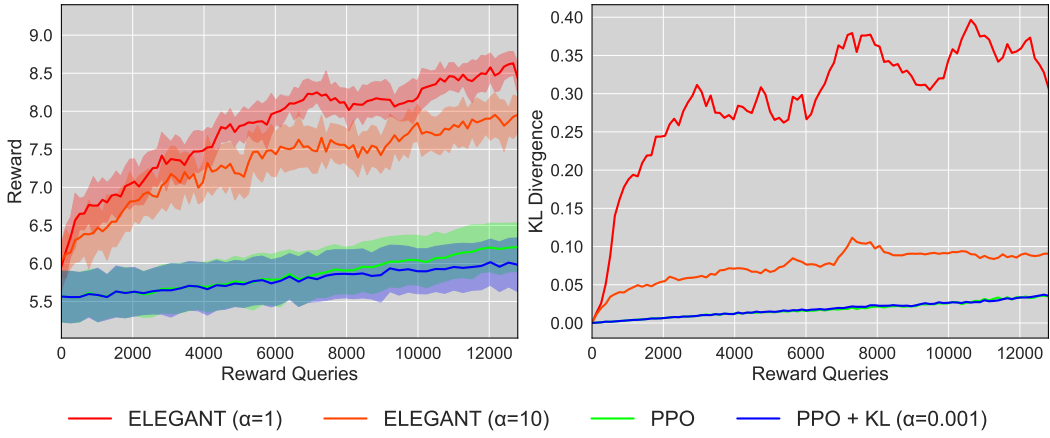


Figure 6: Training curves of reward (left) and KL divergence (right) for **PPO**, **PPO + KL**, and **ELEGANT** for fine-tuning aesthetic scores. The x axis corresponds to the number of reward queries in the fine-tuning process.

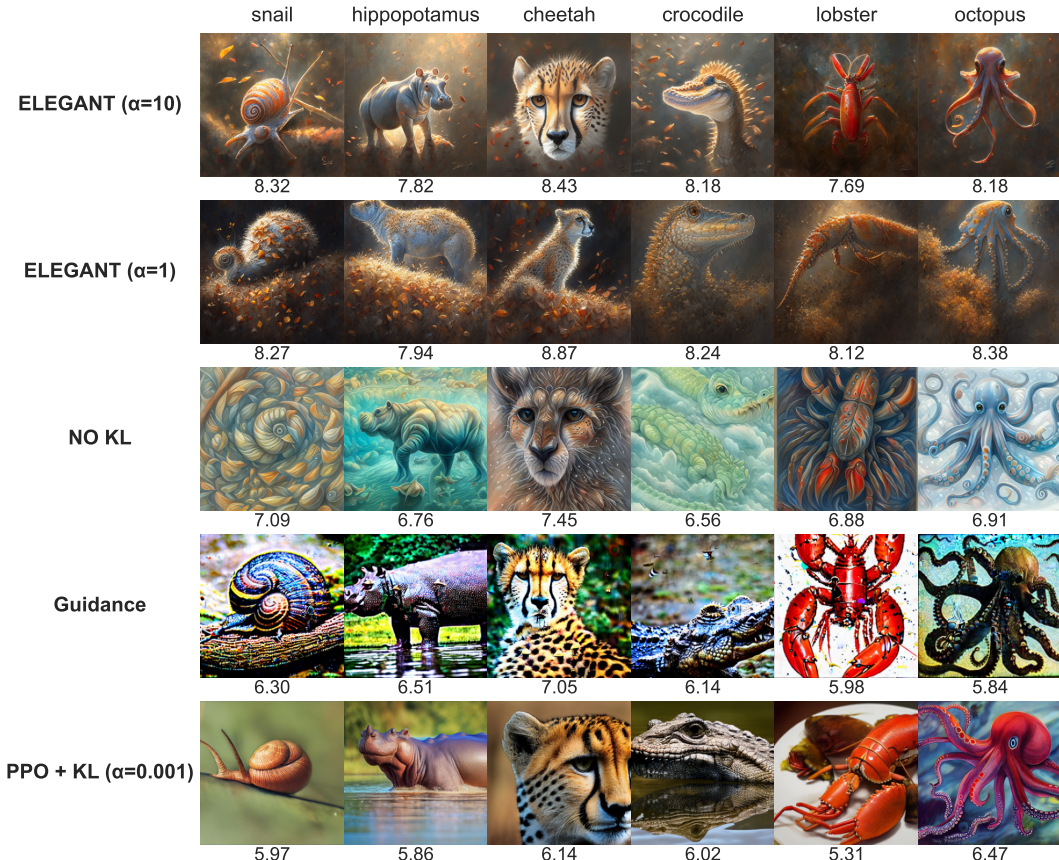


Figure 7: More images generated by **ELEGANT** and baselines. **Guidance** is trained on AVA dataset (Murray et al., 2012). All other algorithms (**NO KL**, **Guidance**, **PPO + KL**, and **ELEGANT**) make 12800 reward inquiries to perform fine-tuning. All evaluation prompts are not seen in training.

Table 9: Results of classifier guidance for aesthetic scores. (·) are confidence intervals. Note the top 5% value is 6.00.

Target (y_{con})	Guidance level (γ)	Reward (r)	KL-Div
7	100	5.69 (0.21)	0.34
10	100	6.02 (0.21)	2.45
16	100	6.32 (0.39)	9.33
10	200	6.41 (0.19)	5.99